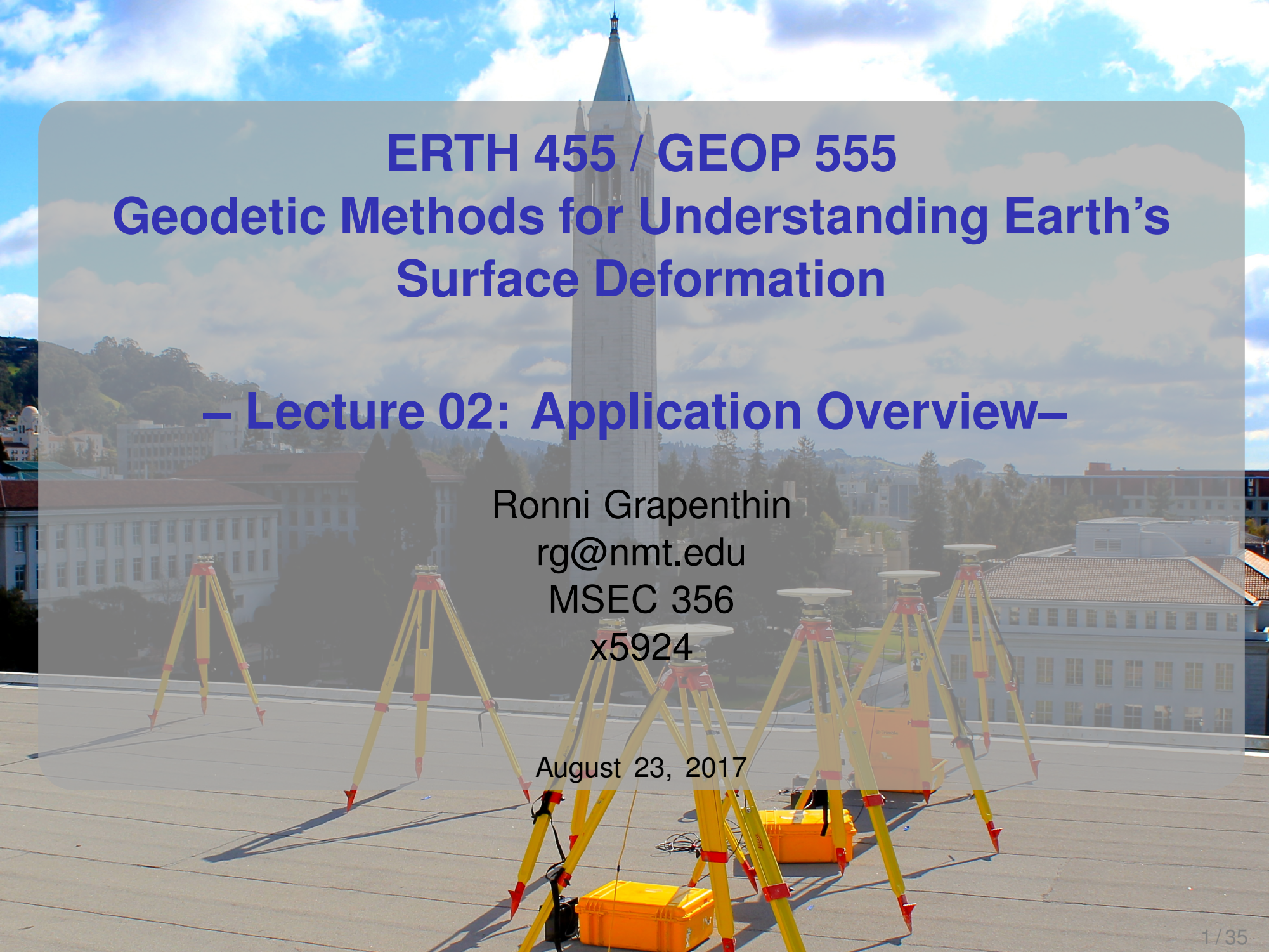

ERTH 455 / GEOP 555
Geodetic Methods for Understanding Earth's Surface Deformation

– Lecture 02: Application Overview–

Ronni Grapenthin
rg@nmt.edu
MSEC 356
x5924

August 23, 2017

Applications – Plate Kinematics

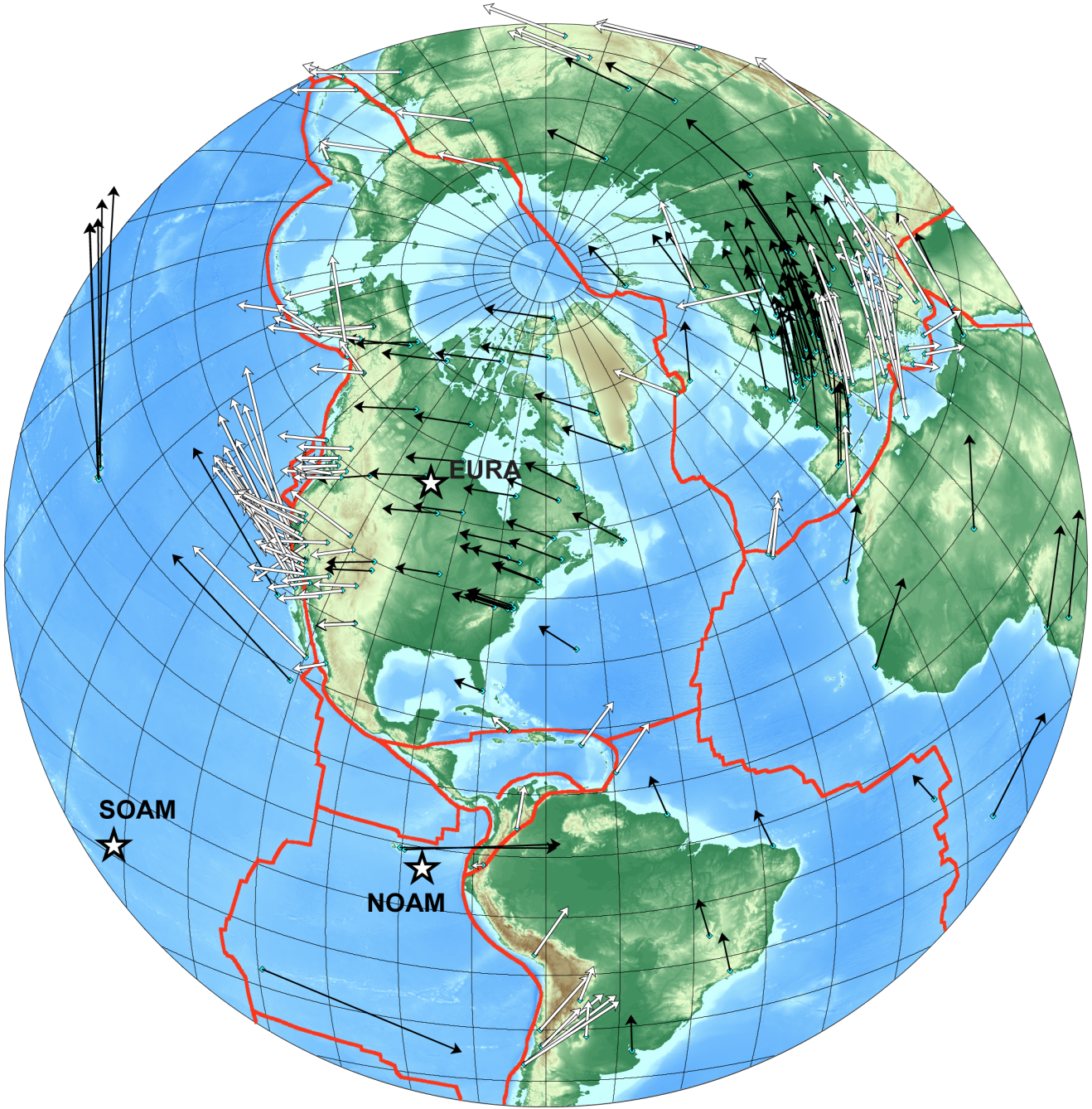

courtesy: Jeff Freymueller, UAF

Reference Frames – ITRF vs. fixed (stable North America)

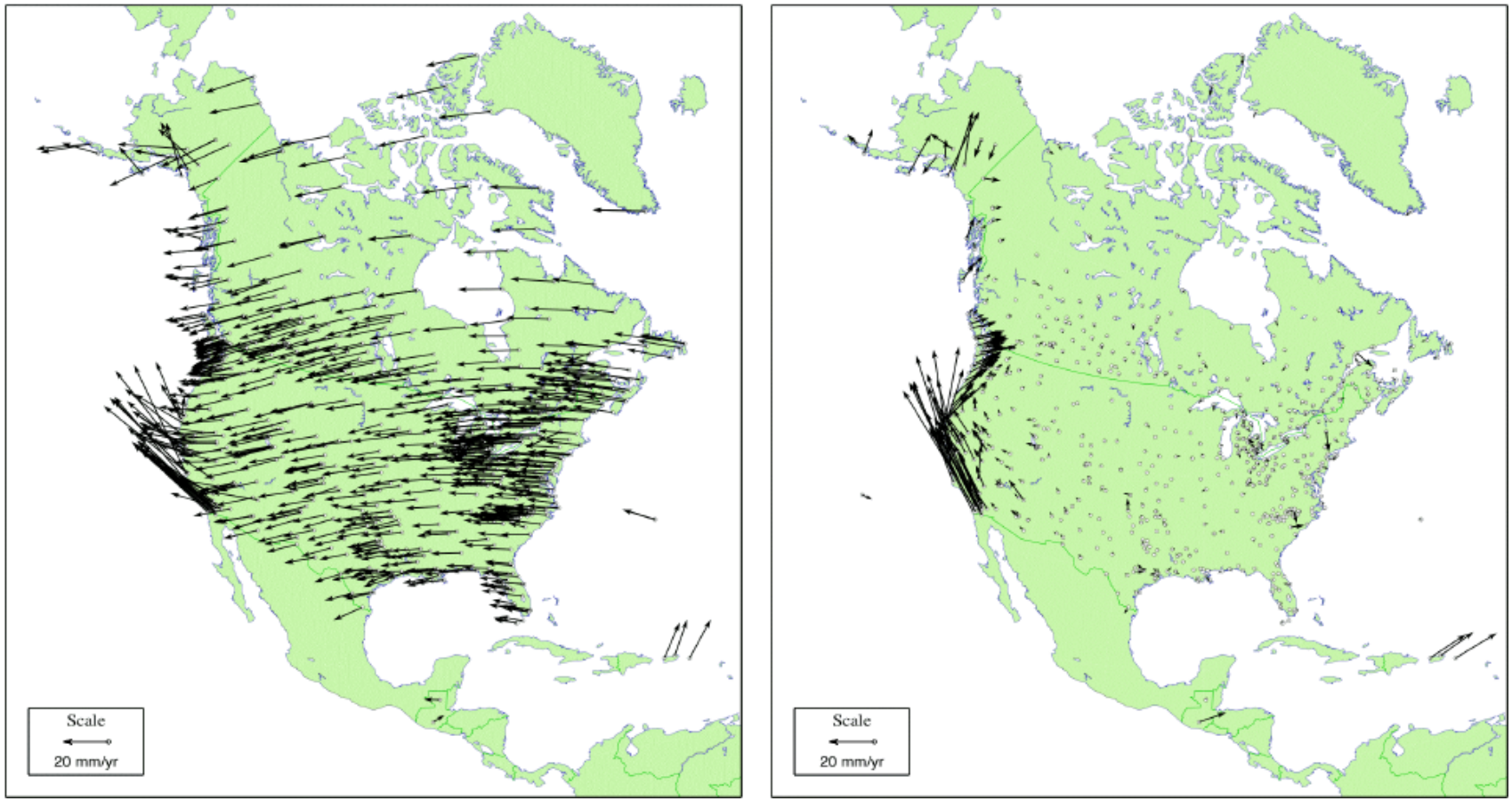

courtesy: Jeff Freymueller, UAF

Reference Frames – Tibet

“Tibetan Plateau Reference Frame”

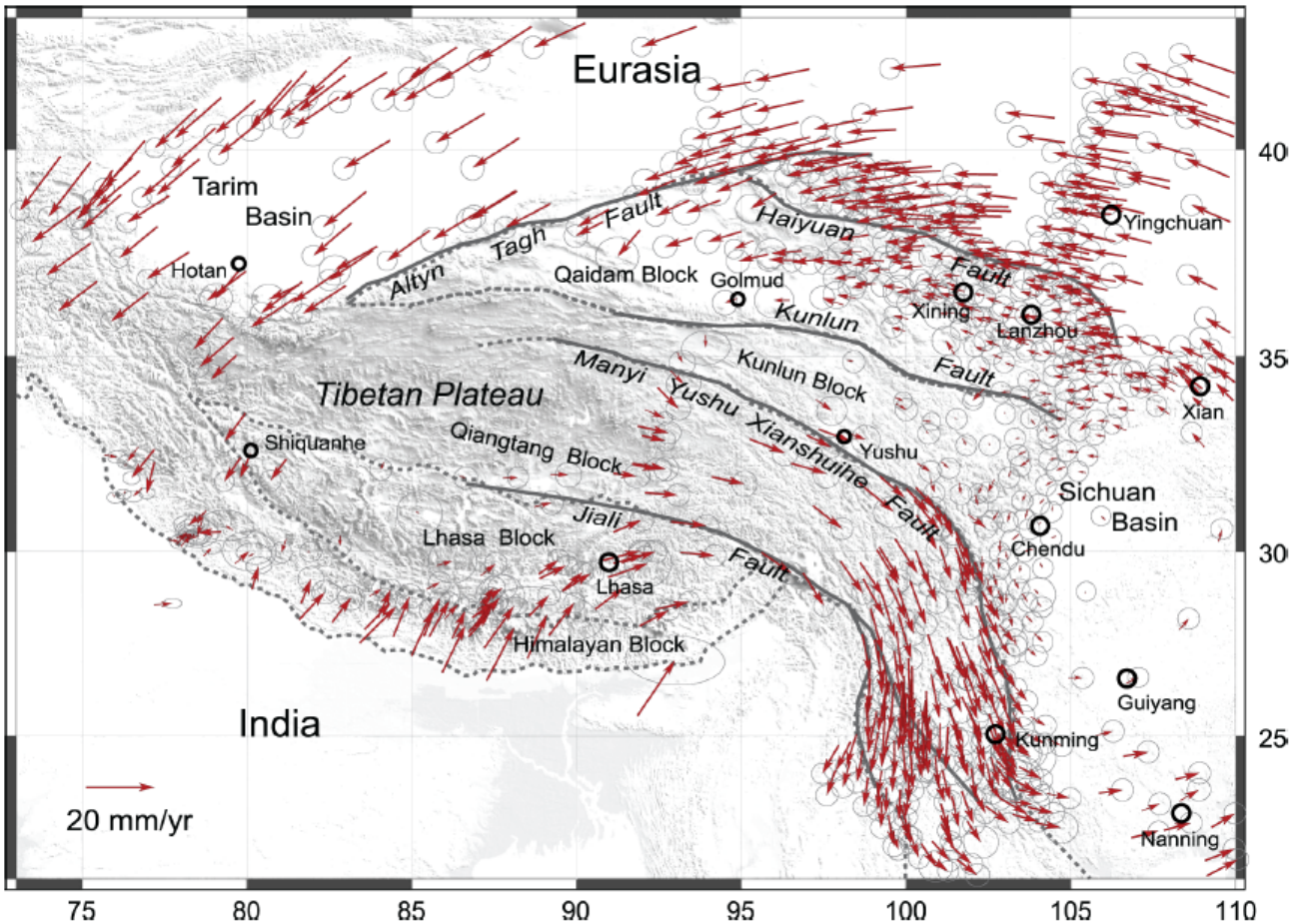

Gan et al. (2007) explained these motions in terms of a series of blocks separated by mostly strike-slip faults ➔ plateau is deforming, but not changing area.

courtesy: Jeff Freymueller, UAF

Applications – Interseismic strain buildup

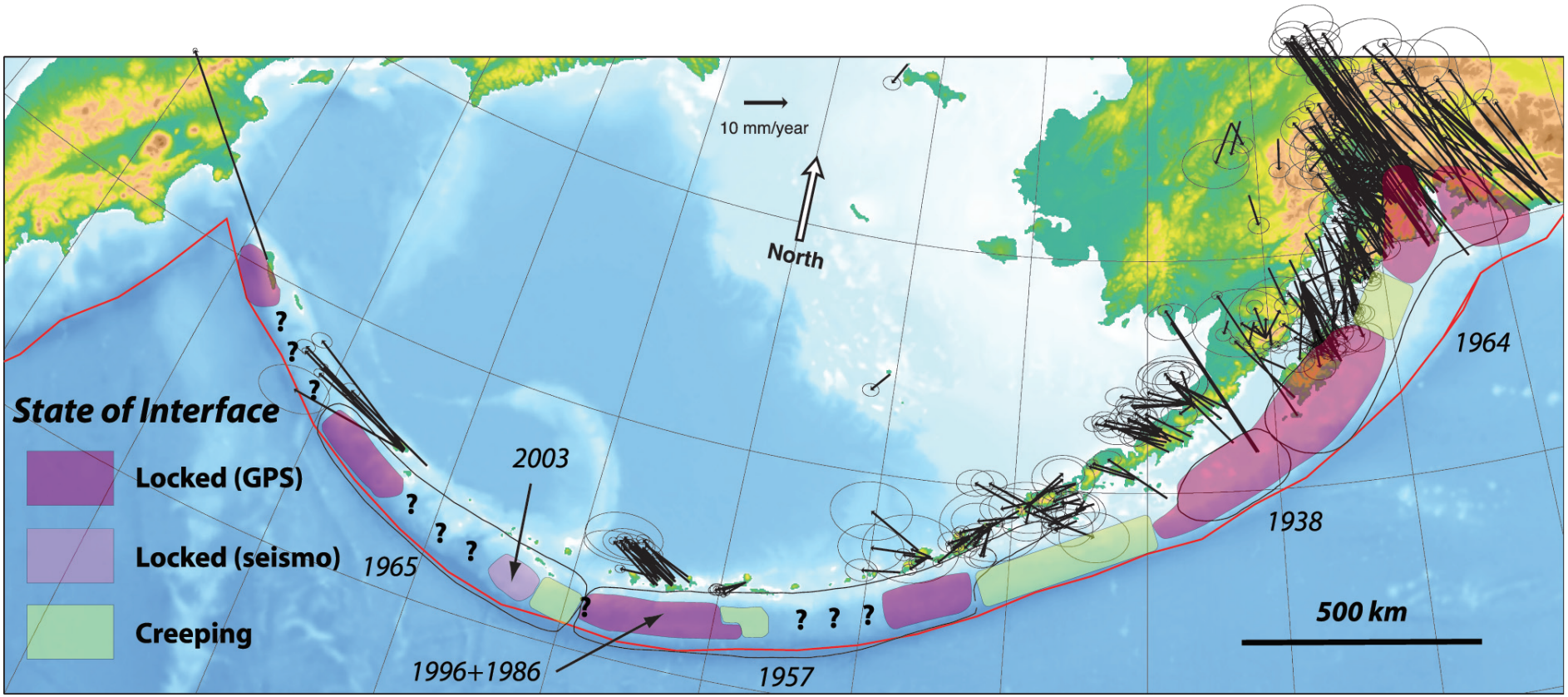

Freymueller et al. 2008, AGU Monograph

Applications – Elastic Fault Deformation

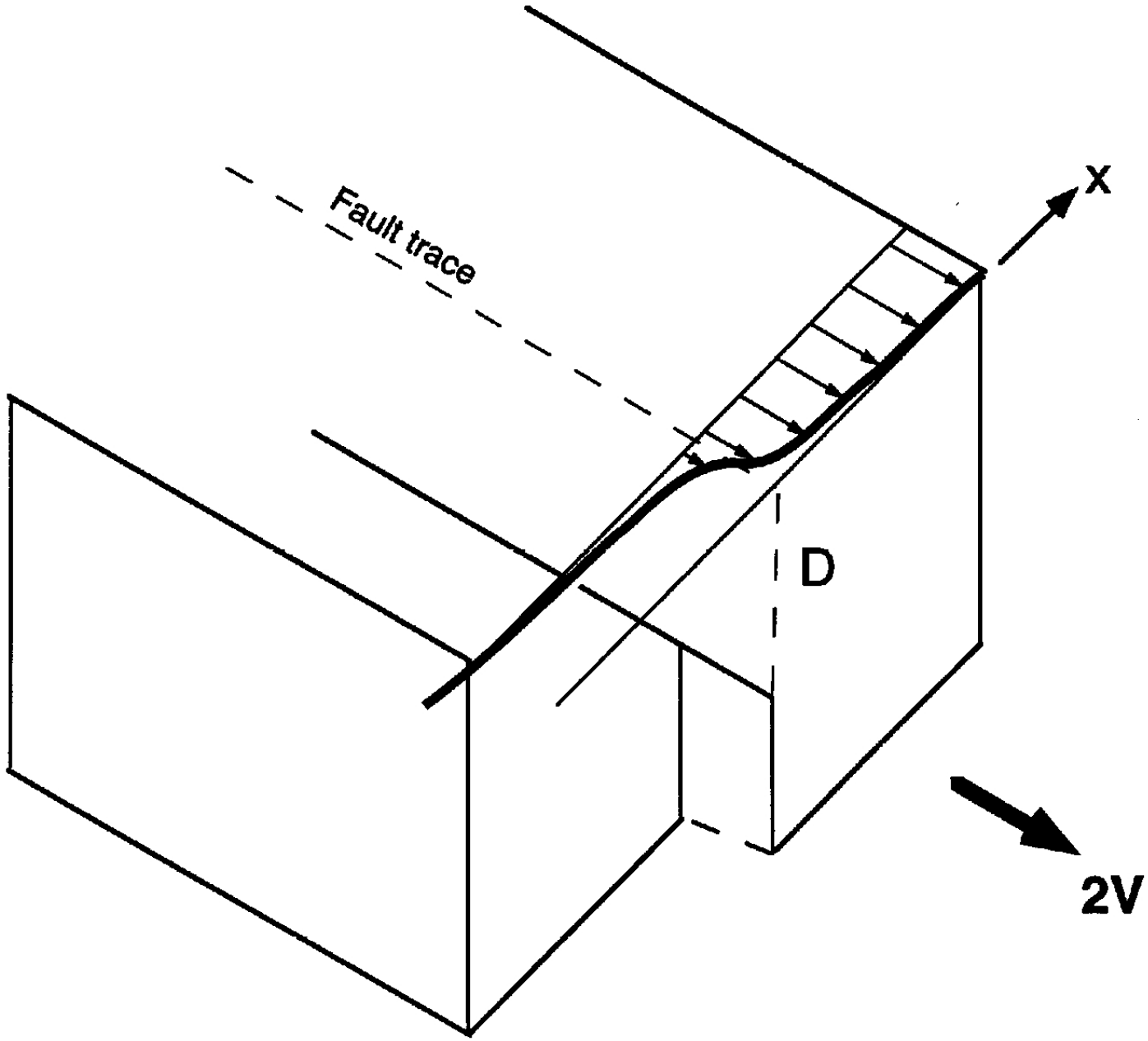

Application – Slip Estimation (2002 Denali)

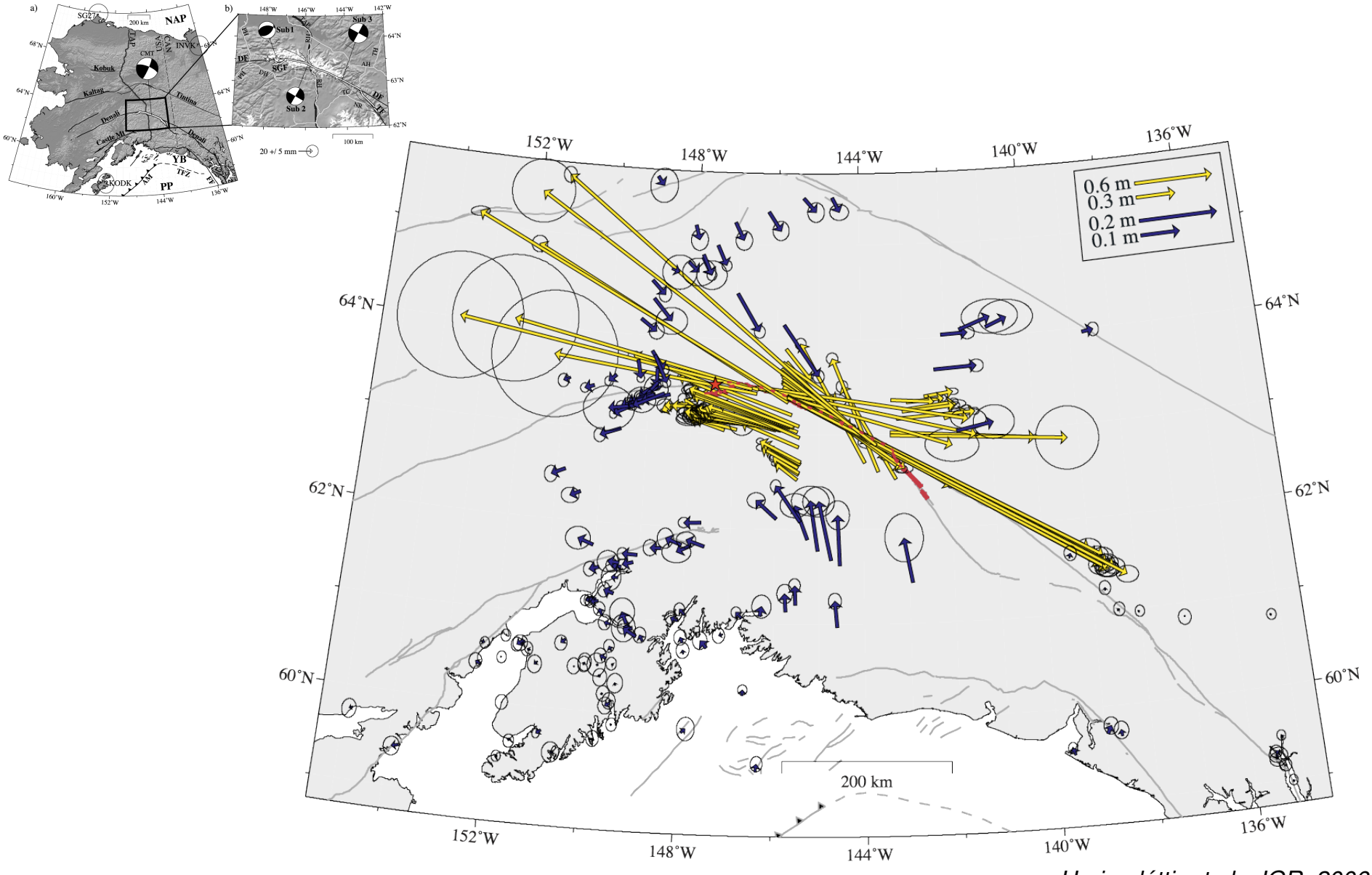

Hreinsdóttir et al., JGR, 2006

2002 M_w=7.9 Denali Earthquake

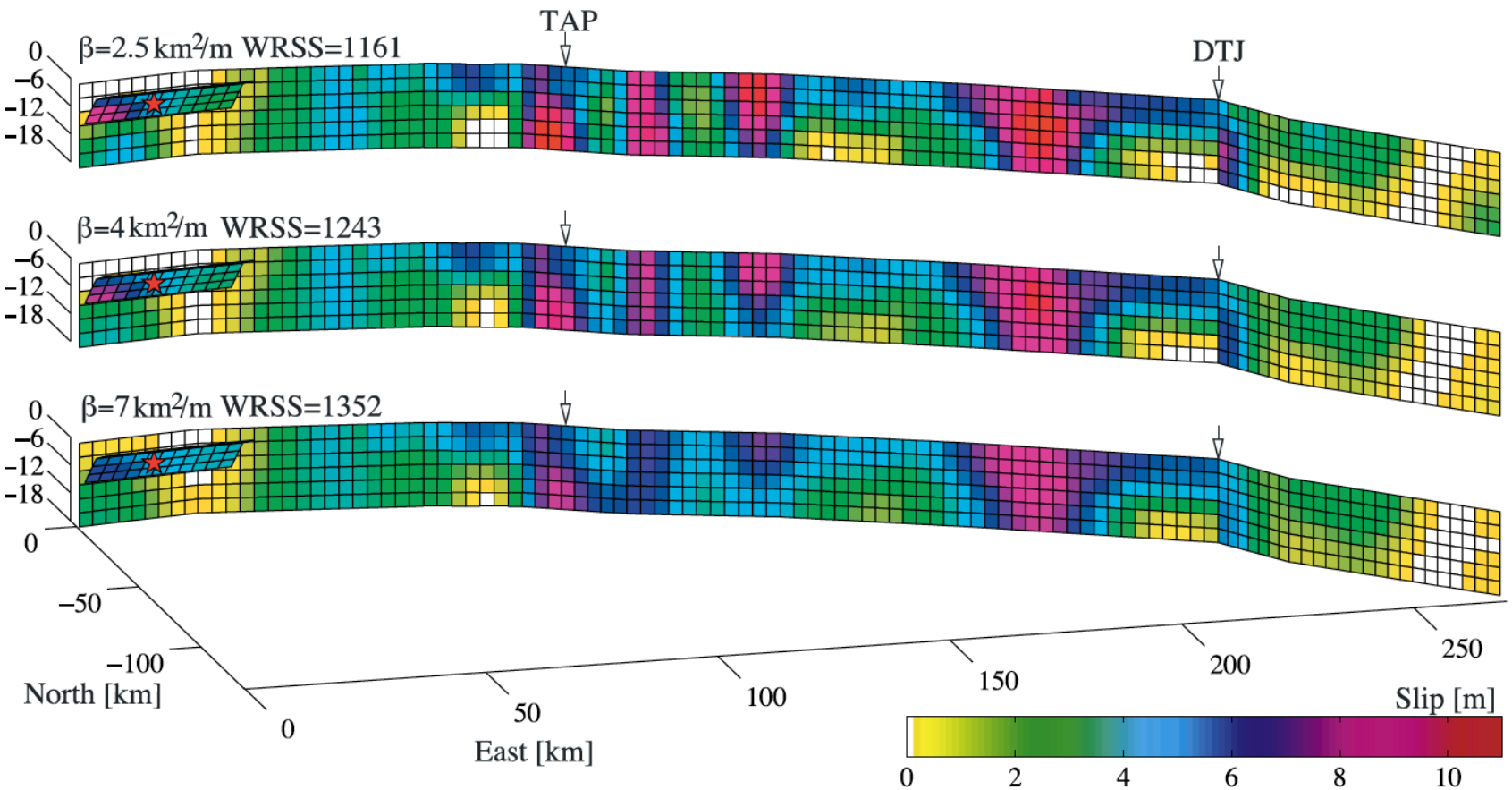

Figure 10. Range of reasonable coseismic slip models from the roughest (β = 2.5 km^2/m) to the smoothest (β = 7 km^2/m). The axes show easting, northing, and depth in km. TAP, Trans-Alaska pipeline; DTJ, Denali-Totschunda fault junction. Red star indicates the Denali Fault earthquake epicenter.

Hreinsdóttir et al., JGR, 2006

Applications – Co-seismic (Tohoku, 2011)

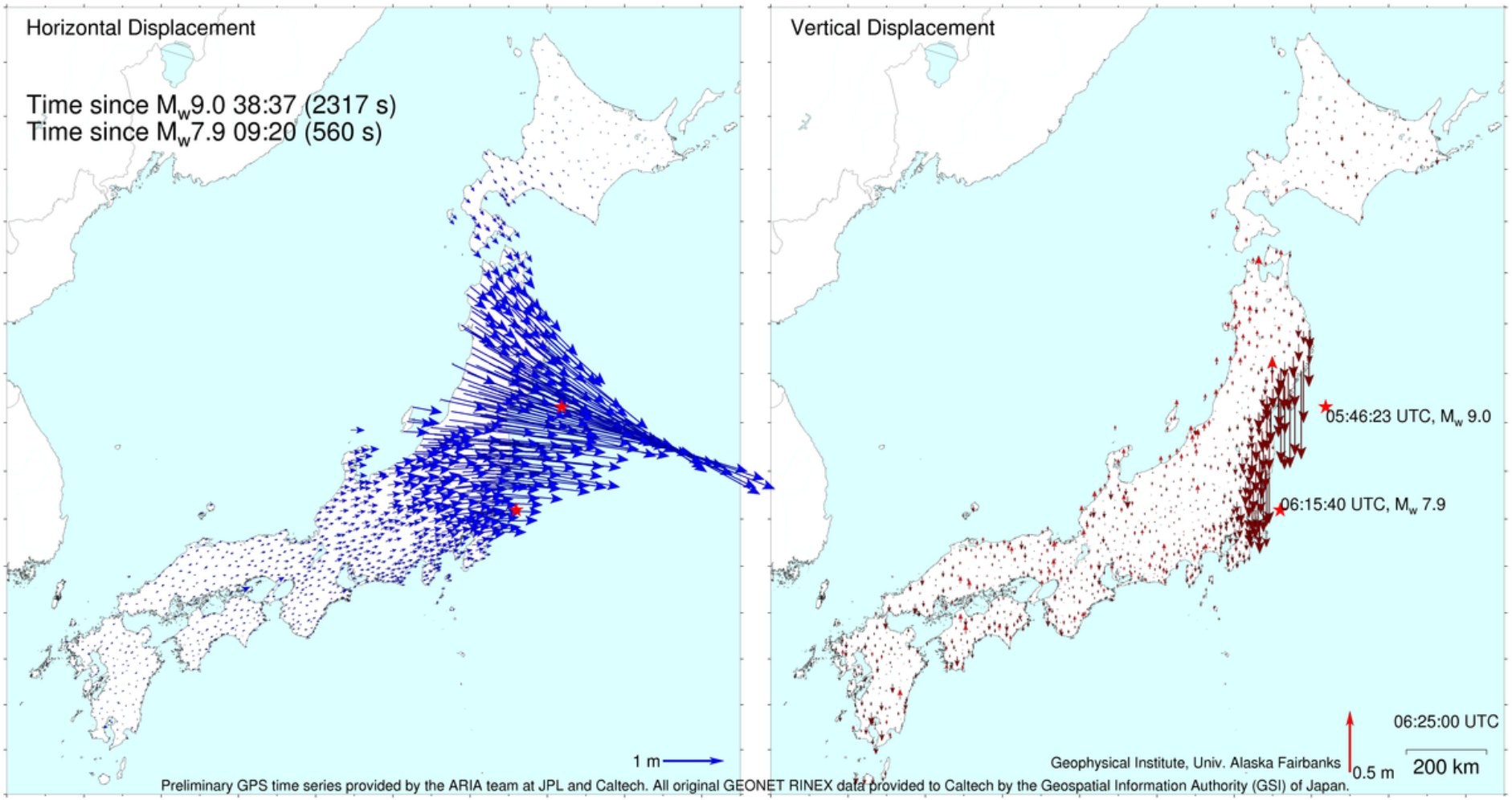

30 seconds per frame

Grapenthin and Freymueller, GRL, 2011

video doesn't work? try: `https://www.youtube.com/watch?v=1QCcVqZgNKw`

Applications – Co-seismic (Tohoku, 2011)

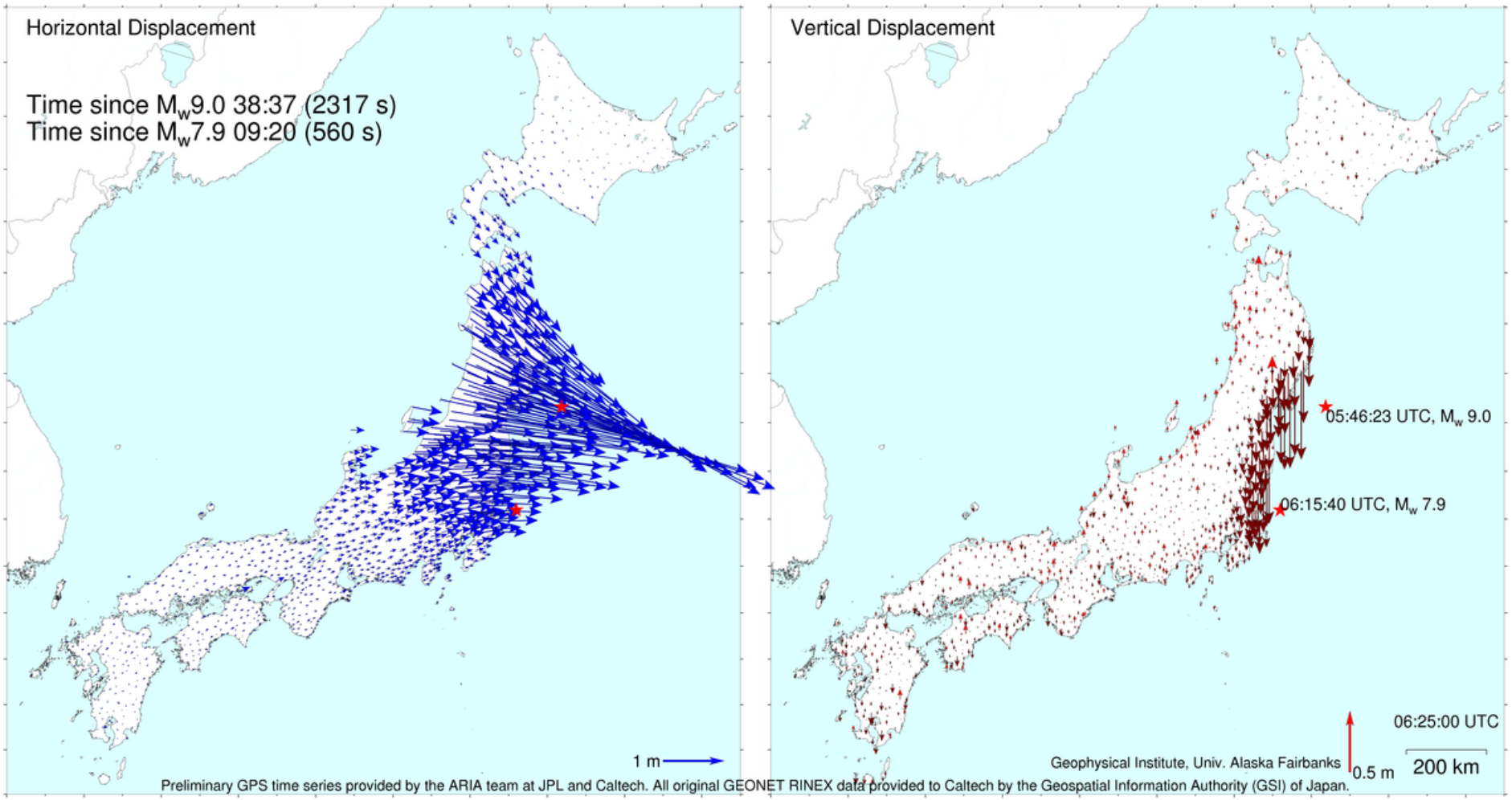

1 second per frame

Grapenthin, 2012

video doesn't work? try: `https://www.youtube.com/watch?v=rMhhyb6Yy94`

Applications – Co-seismic (Gorkha, 2015)

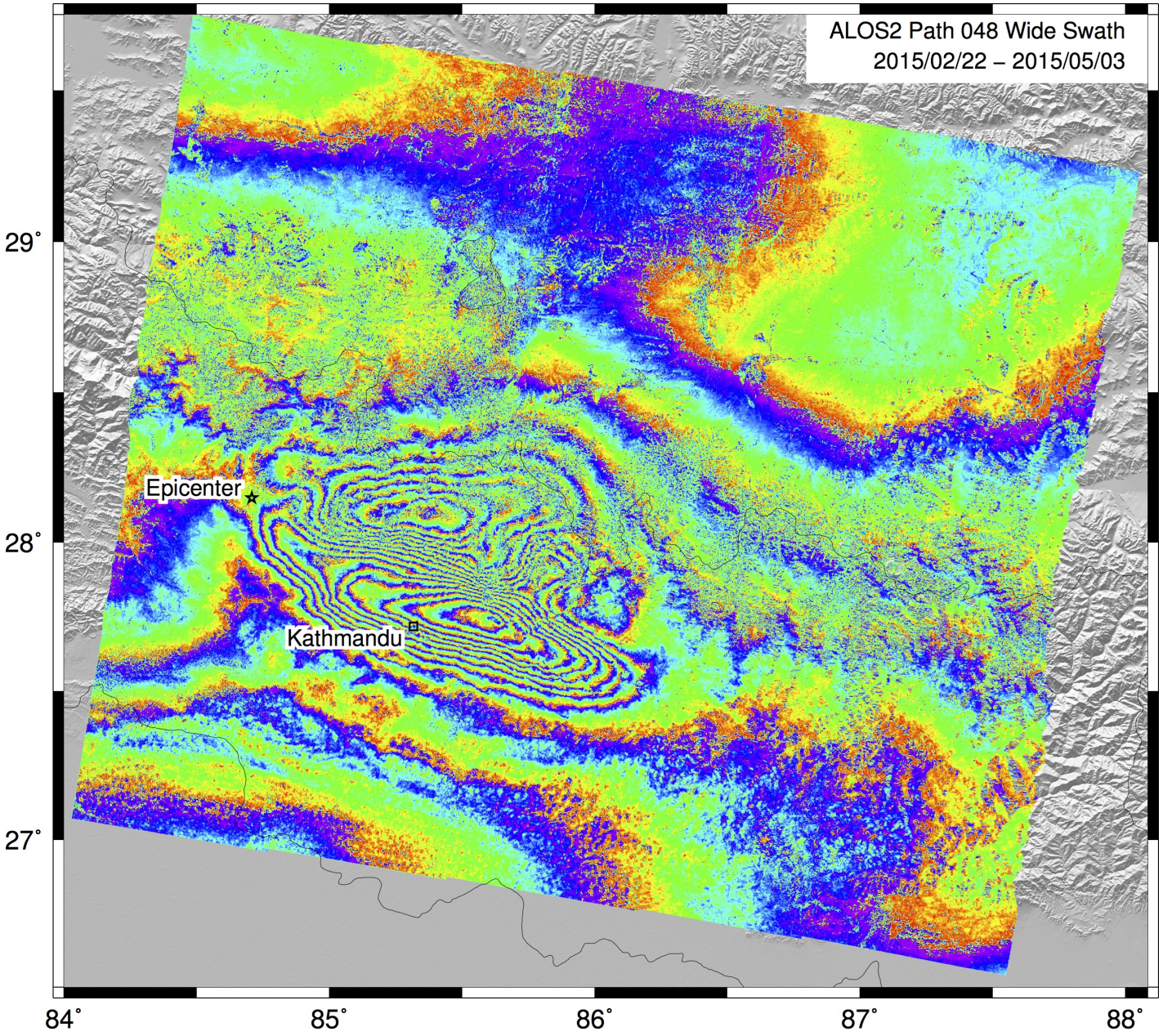

Lindsey et al. 2015, GRL

Applications – Co-seismic (Gorkha, 2015)

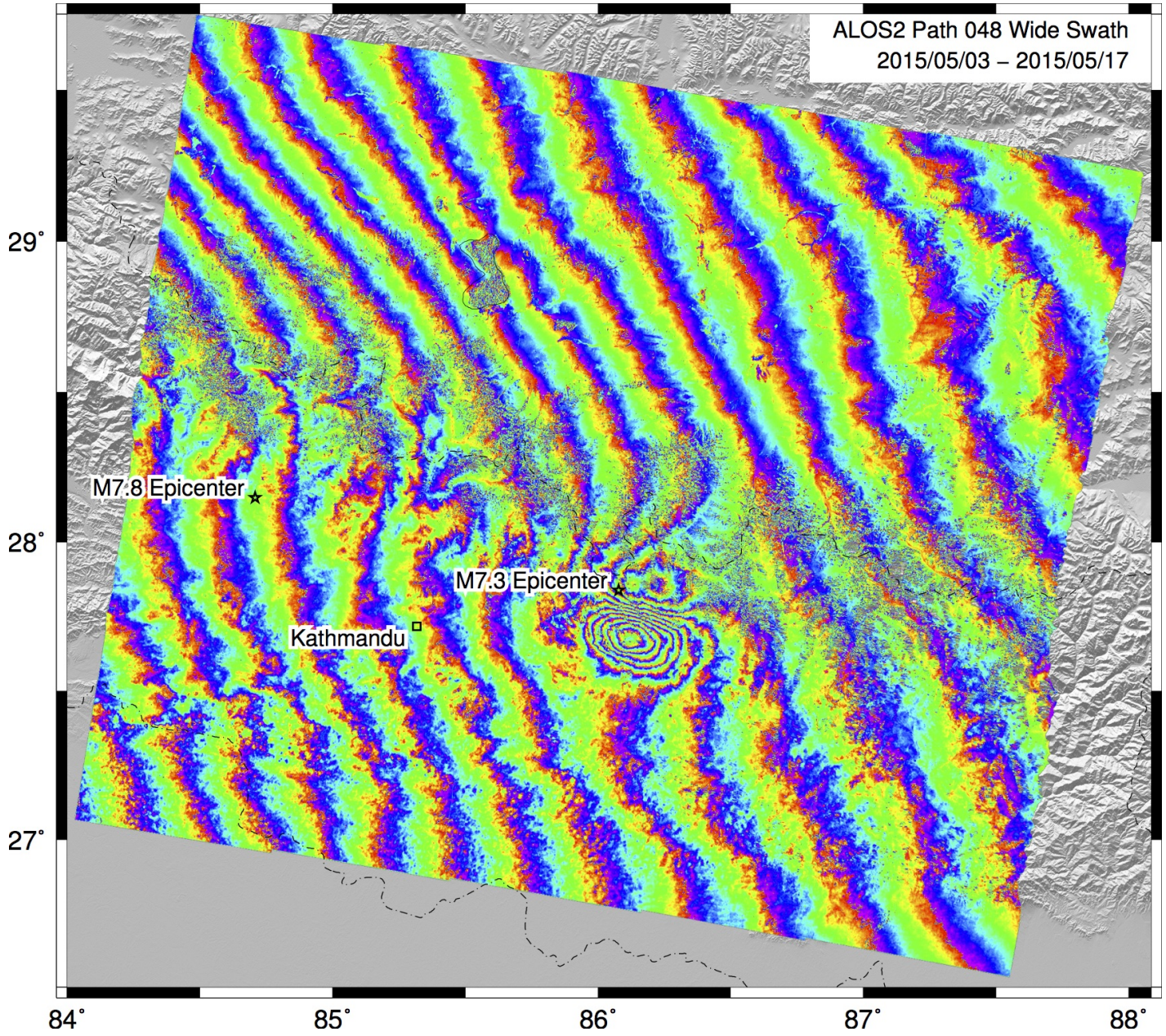

Lindsey et al. 2015, GRL

Applications – Co-seismic (Gorkha, 2015)

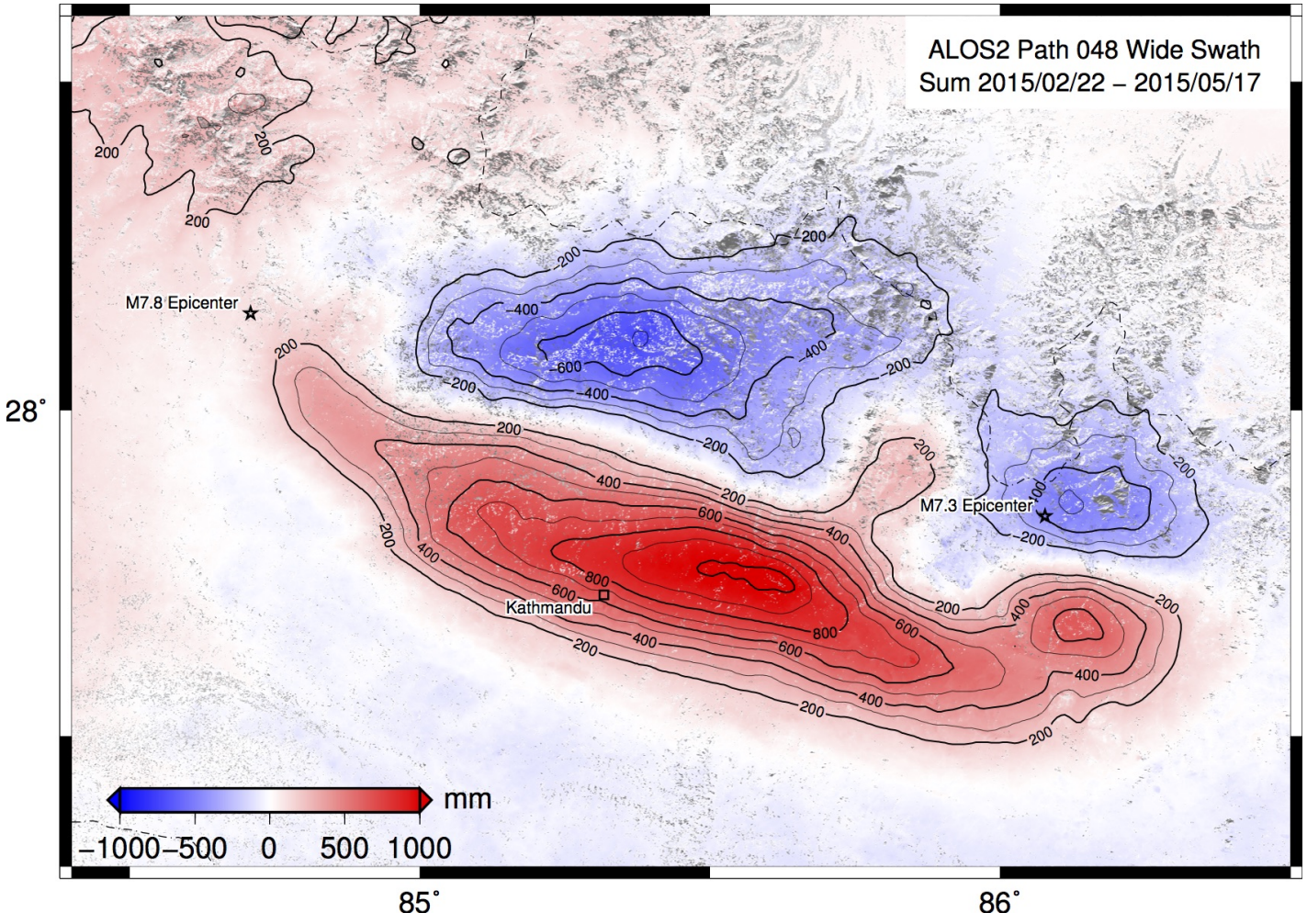

Lindsey et al. 2015, GRL

Applications – Slow Slip

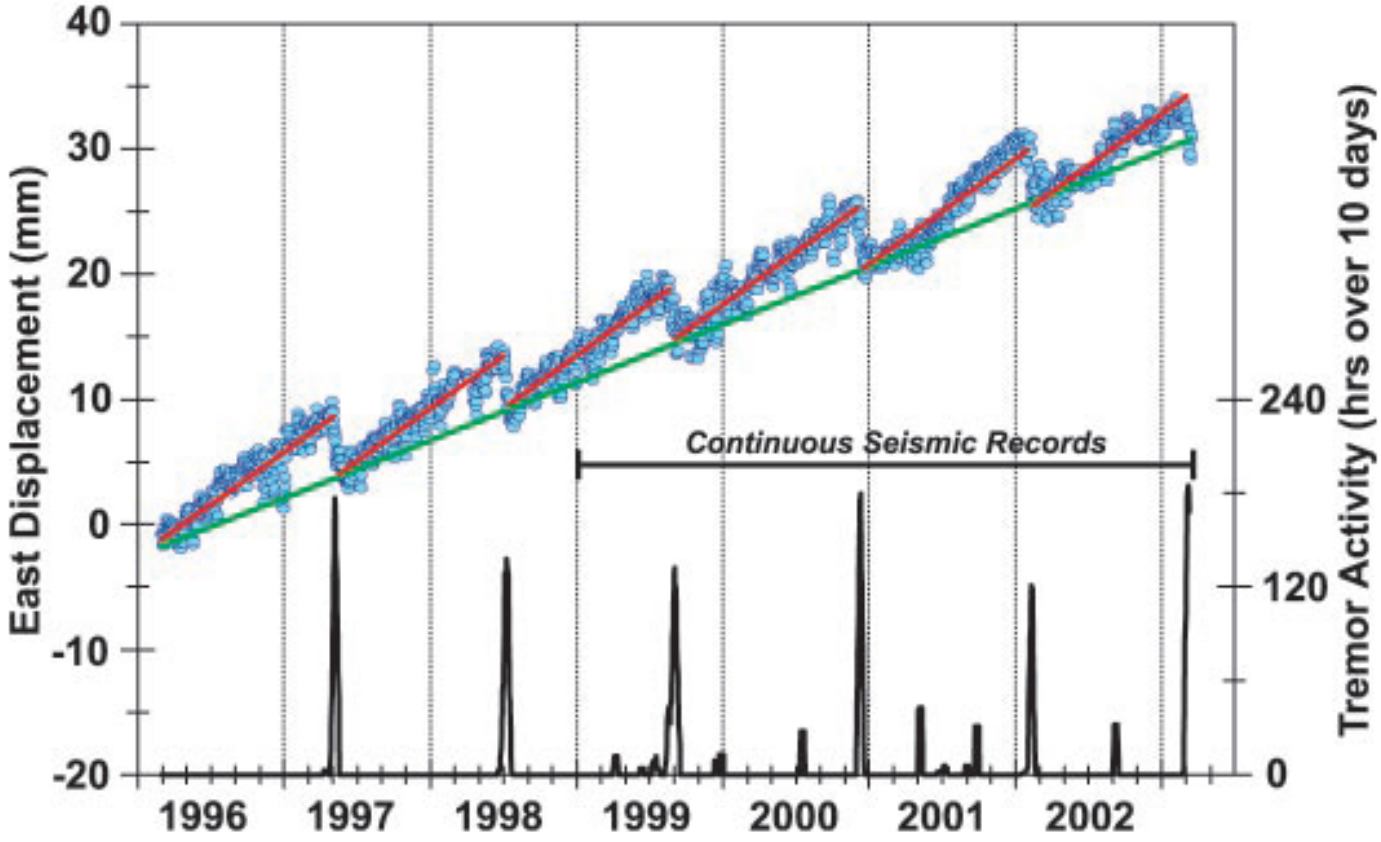

Rogers & Dragert 2003, Science

Applications – Early Warning (2014 South Napa)

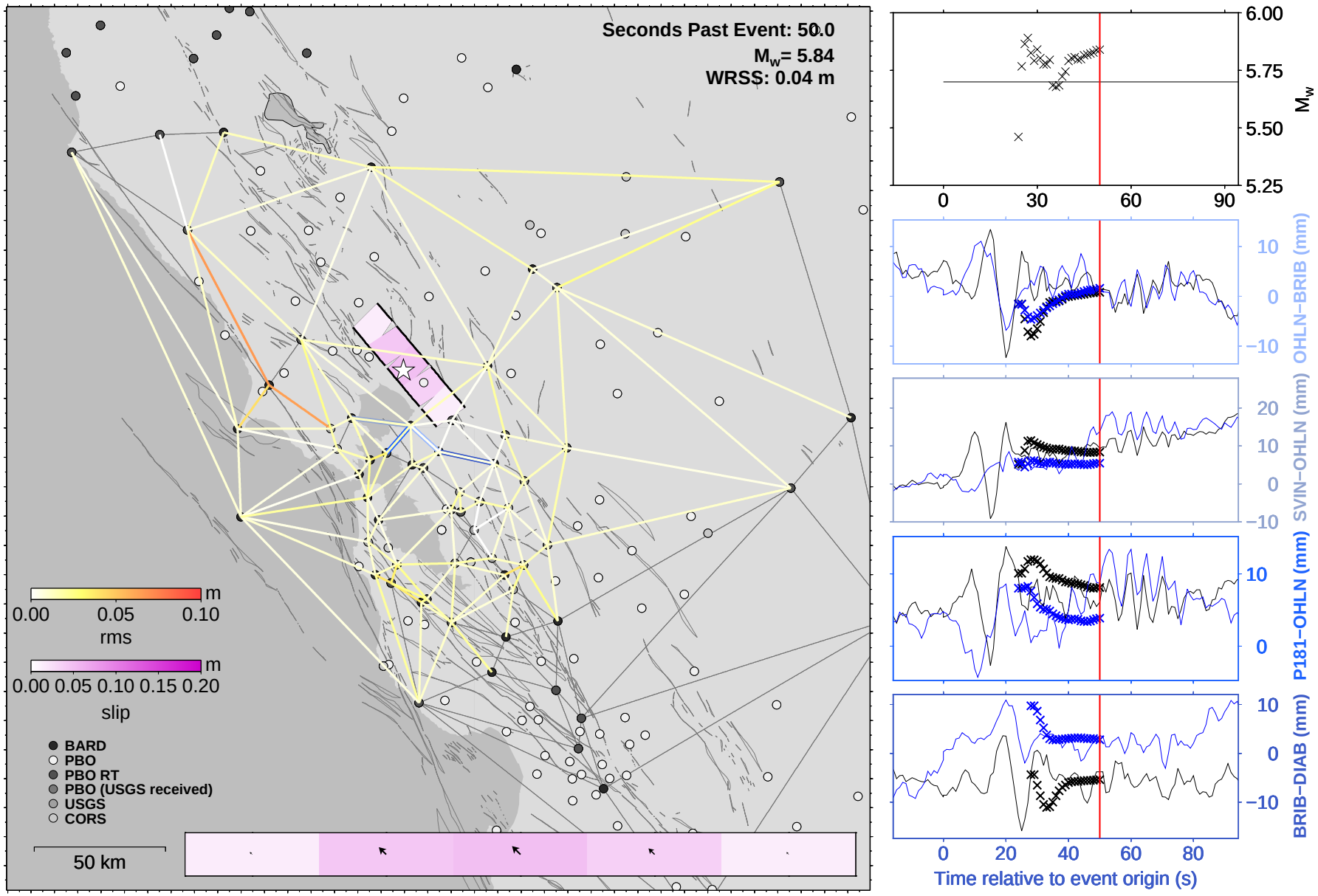

Grapenthin et al. 2014, GRL

Applications – Volcano Hazards

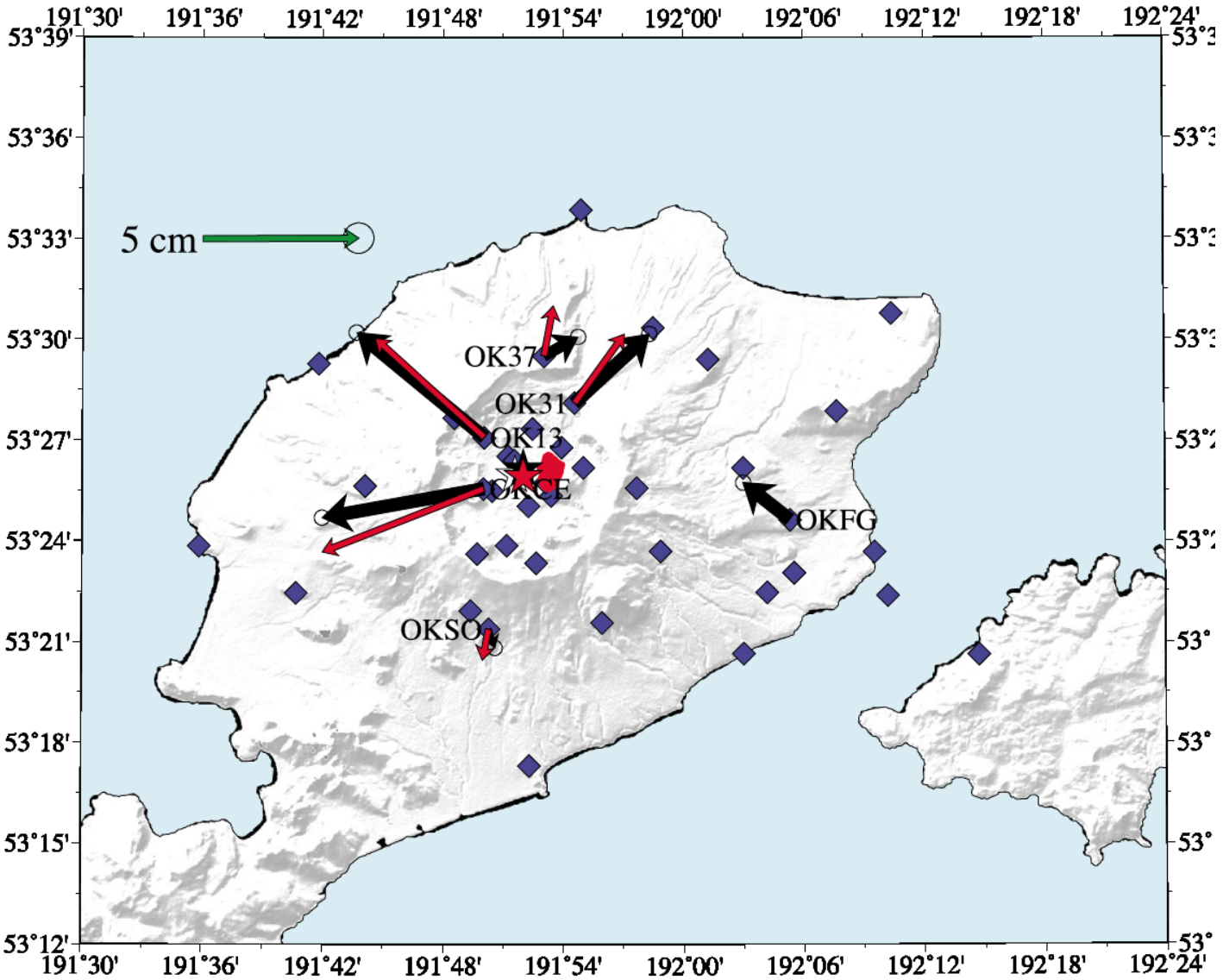

Freymueller & Kaufmann, 2010, JGR

Applications: Volcano Hazards

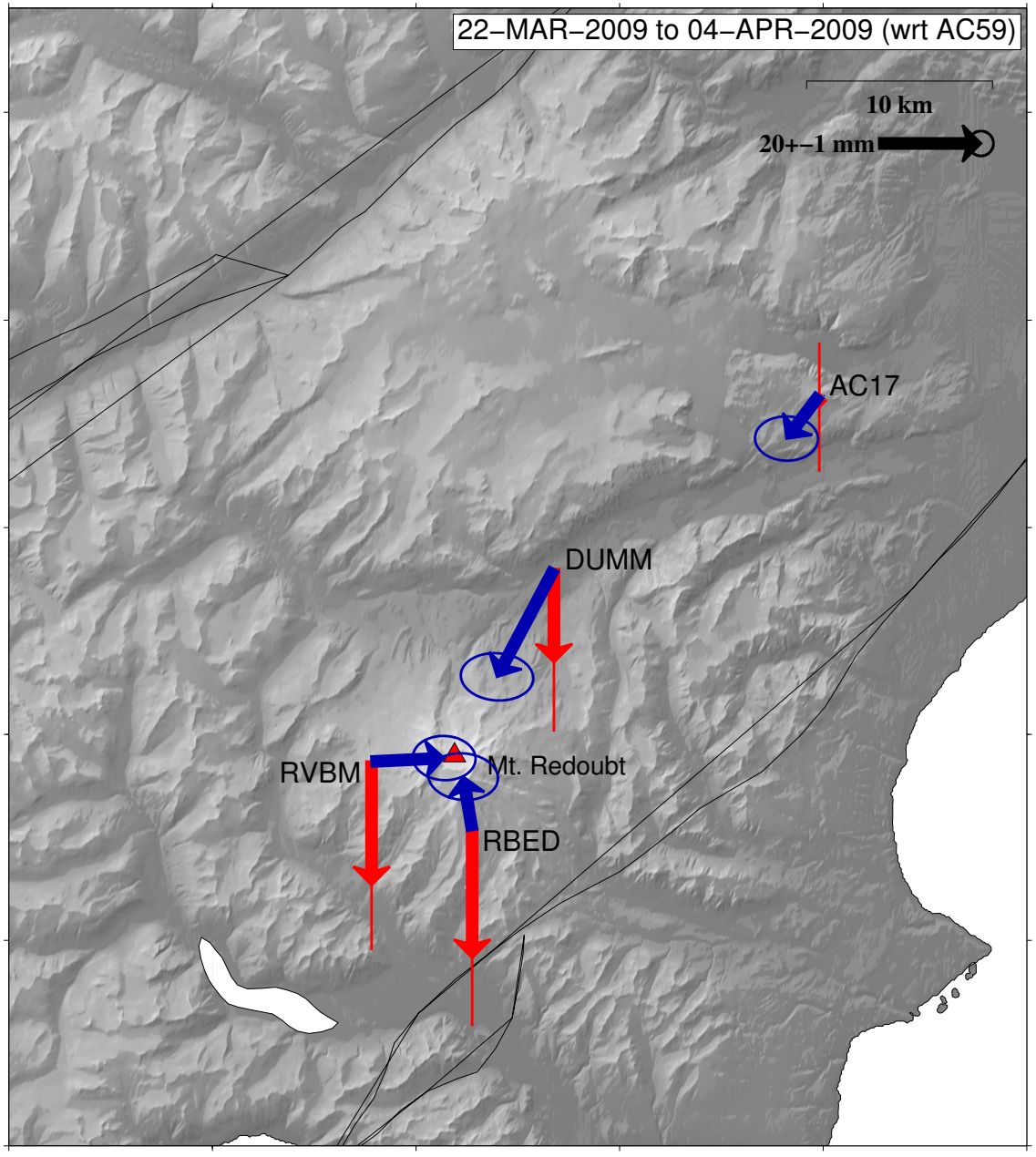

Data
horizontal
vertical

Model
horizontal
vertical

Grapenthin et al., 2012, JVGR

Applications: Volcano Hazards

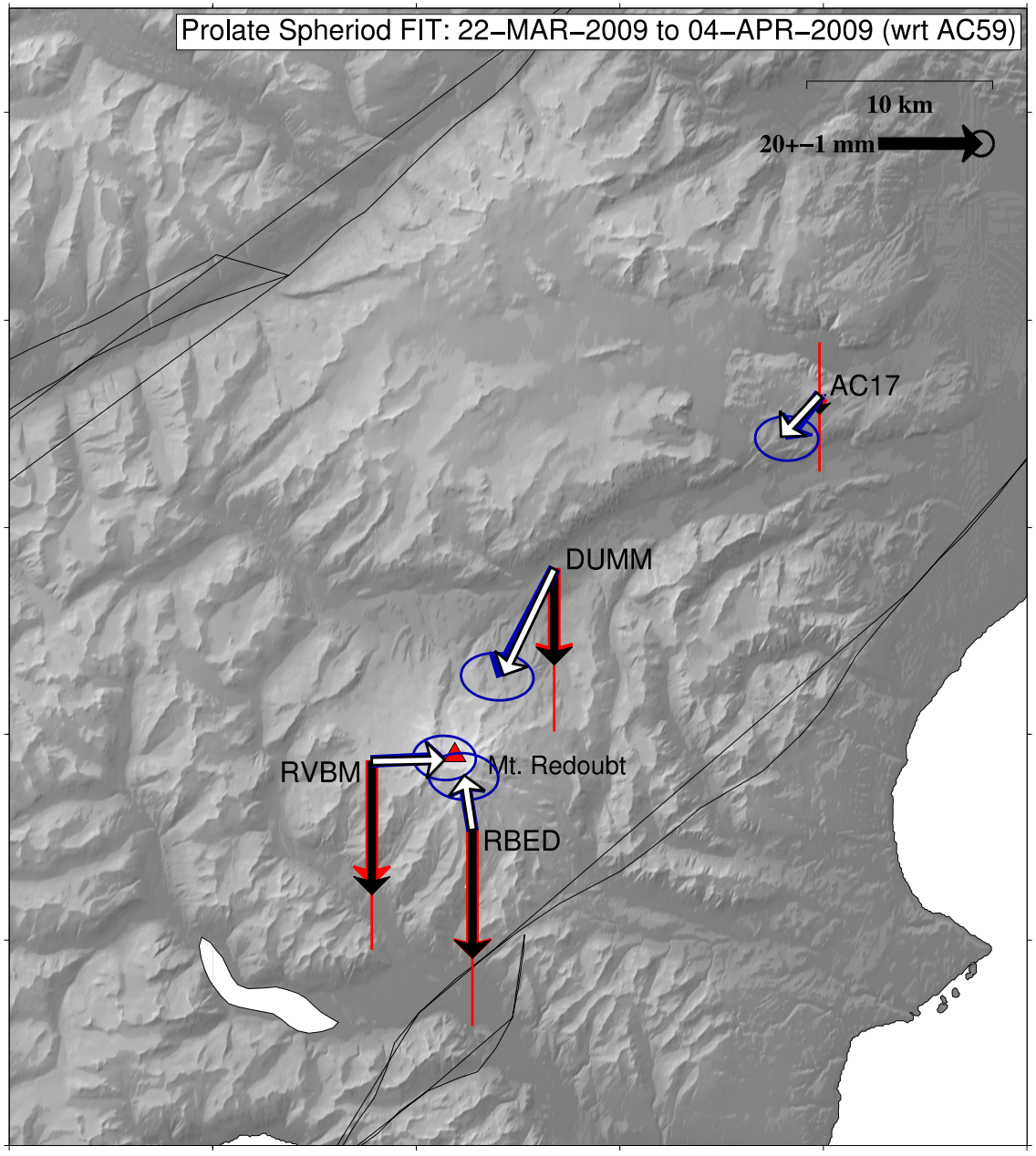

General Spheroid:

$$
\begin{aligned}
r &= 0.5\,km\,\text{E of dome} \\
d &= \mathbf{9.17}\ {}^{6.92}_{15.17}\ km \\
a &= \mathbf{4.50}\ {}^{1.25}_{>10.00}\ km \\
b &= \mathbf{0.475}\ {}^{0.3}_{>4.00}\ km \\
\Delta V &= -(\mathbf{0.05}\ {}^{0.028}_{>0.1})\ km^3
\end{aligned}
$$

F-Test: Spheroid preferred.

Data
horizontal
vertical

Model
horizontal
vertical

Grapenthin et al., 2012, JVGR

Applications – Volcano Hazards

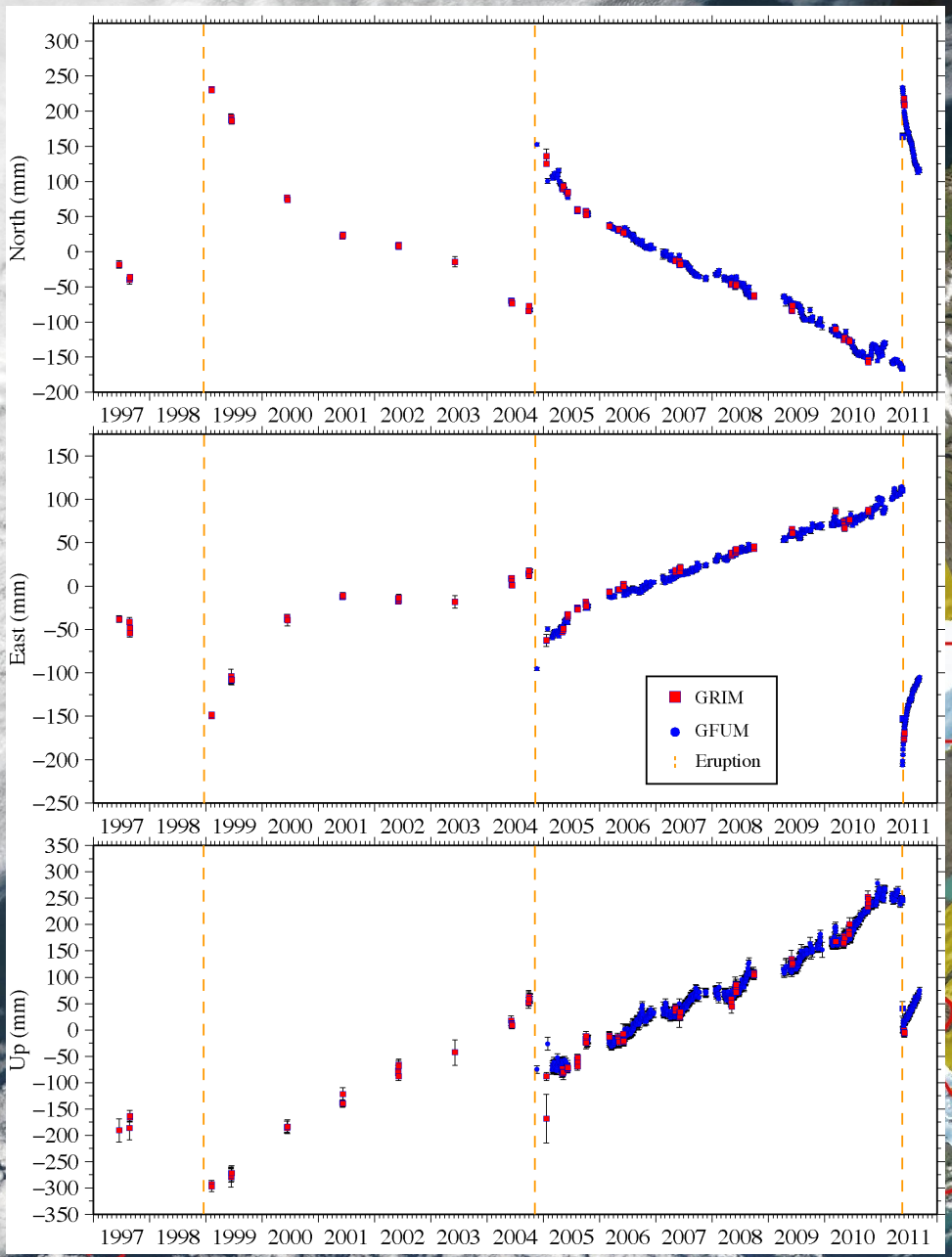

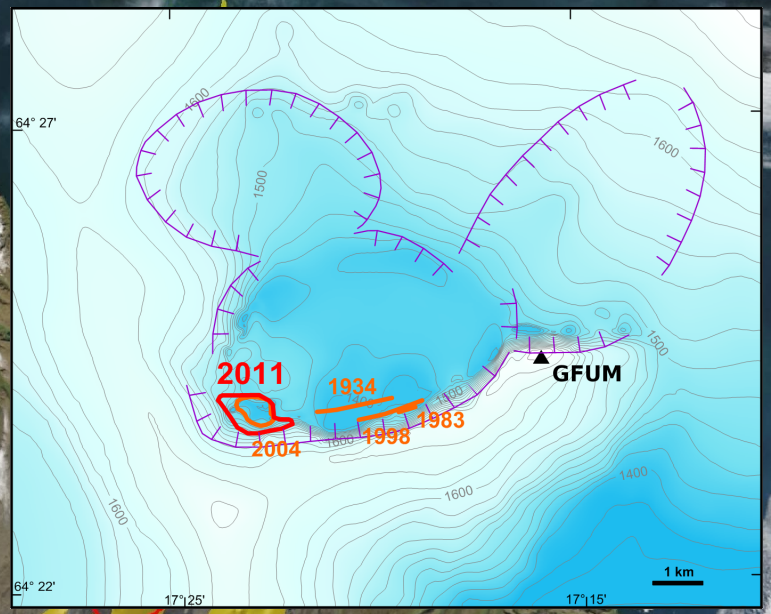

Hreinsdóttir et al. 2011, AGU

Applications – Glacial Isostatic Adjustment

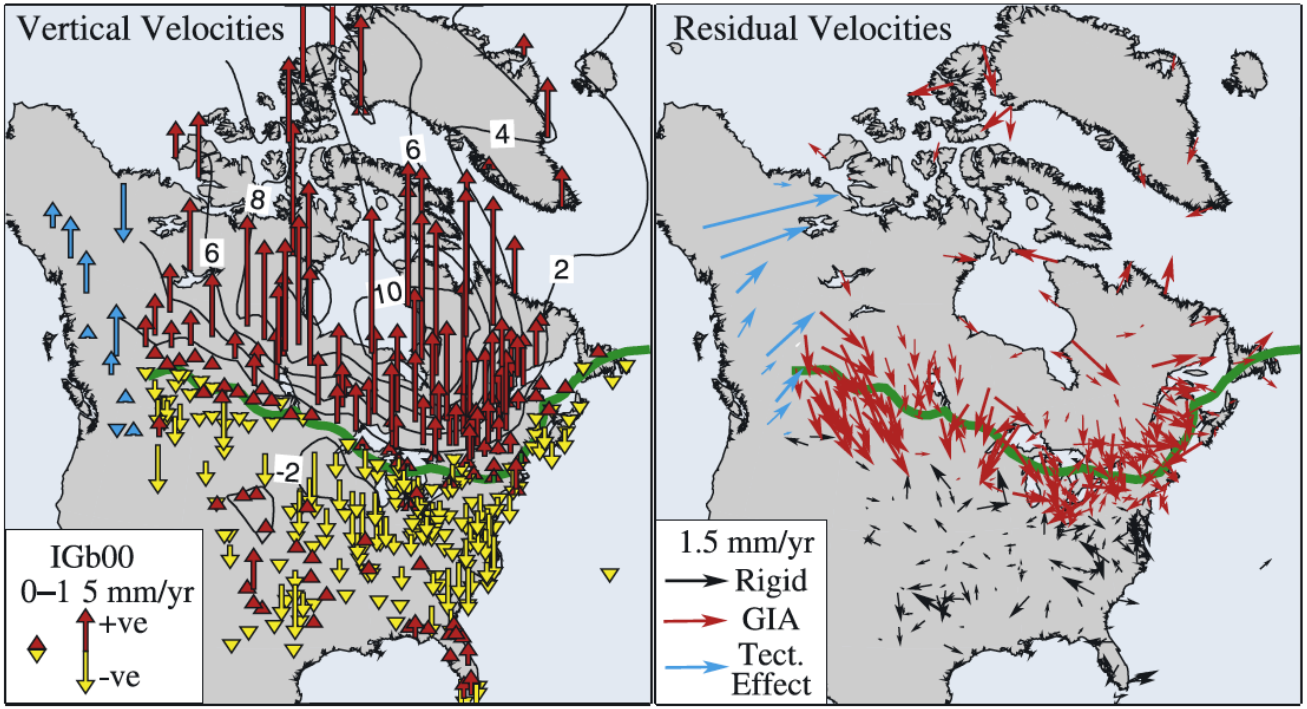

Figure 1. (left) Vertical GPS site motions with respect to IGb00. Note large uplift rates around Hudson Bay, and subsidence to the south. Green line shows interpolated 0 mm/yr vertical "hinge line" separating uplift from subsidence. (right) Horizontal motion site residuals after subtracting best fit rigid plate rotation model defined by sites shown with black arrows. Red vectors represent sites primarily affected by GIA. Purple vectors represent sites that include effects of tectonics.

- estimate rheology
- estimate past ice loads and distribution

Sella et al. 2007, GRL

Applications – Aquifers

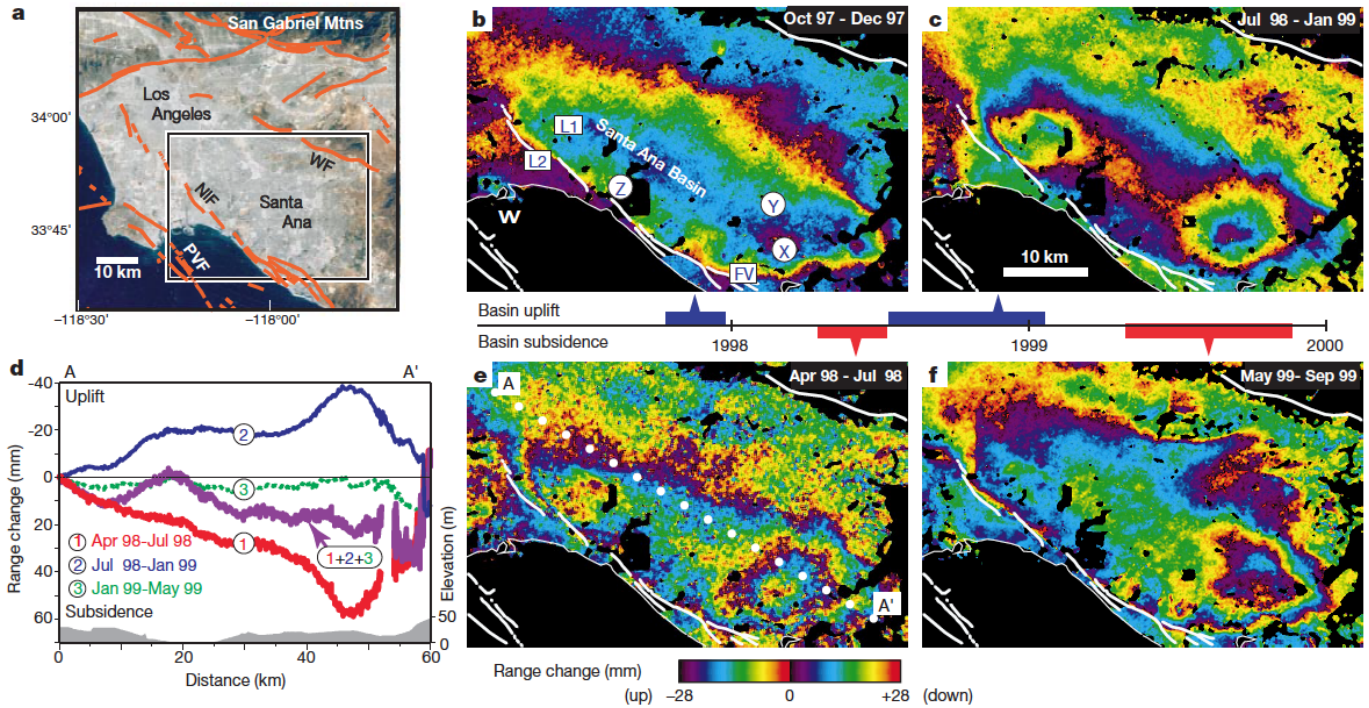

igure 1 Seasonal deformation in the Santa Ana basin. **a**, Location map for iterferograms in **b**, **c**, **e** and **f** (box), and for Figs 2 and 5 (full frame). Faults: PVF, Palos erdes; NIF, Newport–Inglewood; and WF, Whittier. Differential interferograms (**b**, **c**, **e** nd **f**) were constructed by taking the phase difference of paired synthetic aperture radar SAR) images[17], correcting for the topographic contribution using a United States eological Survey digital elevation model and for orbital errors by removing a best-fit lane. The interferograms represent line-of-sight range changes between the surface and atellite. One cycle in colours from red through violet represents a decrease in the range of 8 mm between the ground and the satellite. The time history bar in the centre of the gure shows the period that each image spans, and summarizes the type of motion bserved in the Santa Ana basin. Blue bar denotes uplift (winter months) and red bar denotes subsidence (summer). **b**, October 1997 to December 1997. This 70-day image shows up to 34 mm of uplift in the Santa Ana basin. W, Wilmington oil field; L1, L2 and FV are GPS sites; and X, Y and Z locate water wells. **c**, July 1998 to January 1999 (175 days). The regions of maximum uplift are at the northwestern and southeastern ends of the basin, with 30 and 50 mm of uplift respectively. **e**, April 1998 to July 1998 (105 days). **f**, May to September 1999 (105 days). The maximum subsidence is 60 mm. Two regions show up to 60-mm subsidence. **d**, Unwrapped range-change profiles along the Santa Ana basin, where unwrapping corrects for phase discontinuities as the phase cycles through increments of 2. Profile location A–A′ is shown as a dotted line in **e**. The deformation is independent of topography, and is thus not an artefact of elevation-dependent atmospheric delays or an inaccurate digital elevation model.

Bawden et al. 2001, Nature

Applications – Aquifers

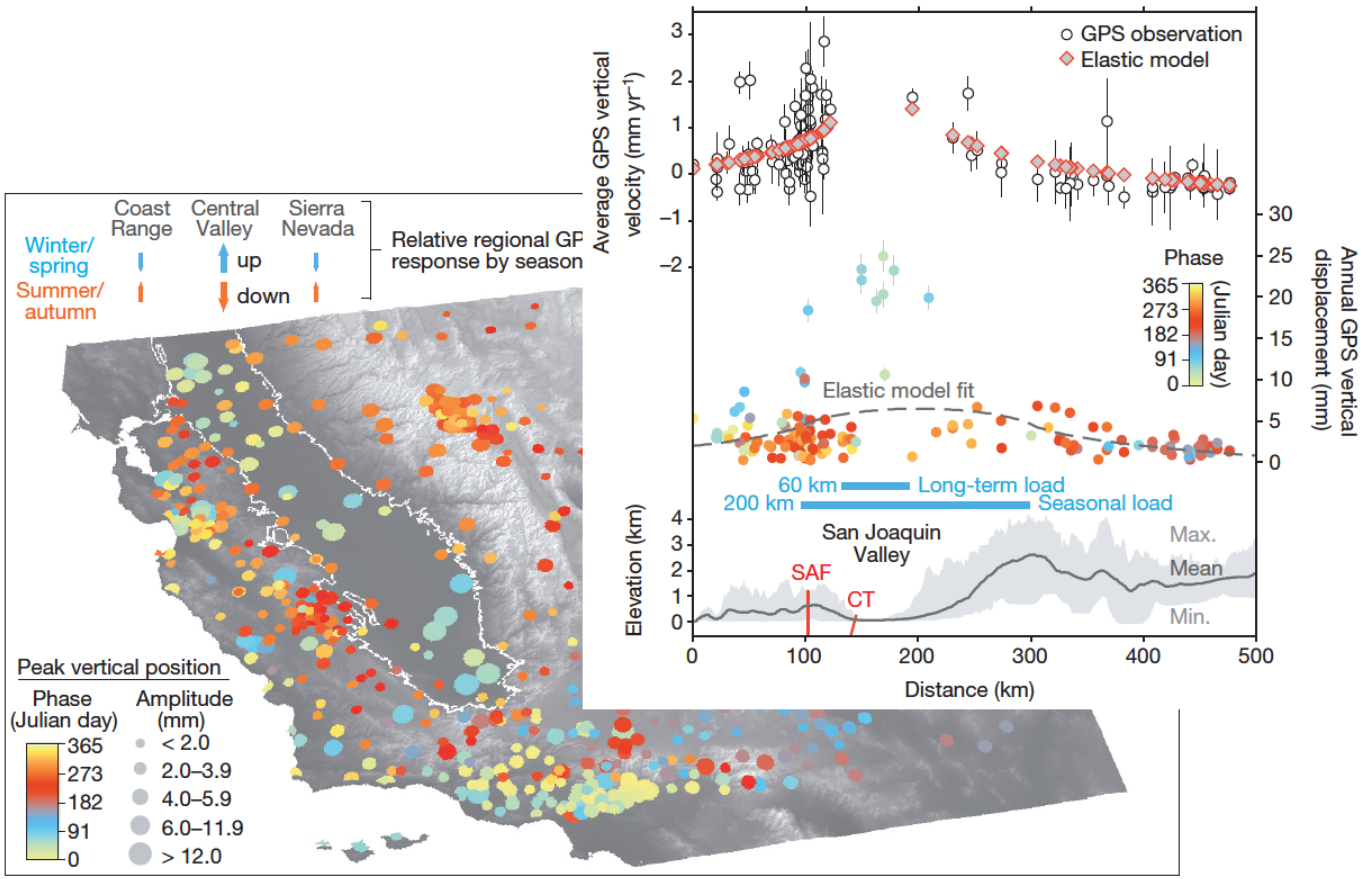

Figure 3 | Seasonal peak uplift from GPS. Phase and peak-to-peak amplitude of annual vertical GPS displacement for all stations included in our analysis. The inset shows histograms of peak uplift phase (binned by month) for stations in the San Joaquin Valley, Sierra Nevada, and Coast Range. Peaks in seismicity rate for the locked and creeping San Andreas Fault at Parkfield are defined as months with higher than average declustered seismicity[6]. Smaller-amplitude peak uplift in the Sierra Nevada and Coast Range during the dry summer and autumn is largely out of phase with larger-amplitude uplift in the San Joaquin Valley driven by the poro-elastic response to recharge during the wetter winter and spring. Stations peripheral to the valley show uplift patterns in accordance with nearby sites on bedrock, indicating the dominance of surface loads in driving vertical motions away from areas affected by local irrigation and groundwater fluctuations.

Amos et al. 2014, Nature

Applications – Snow Load

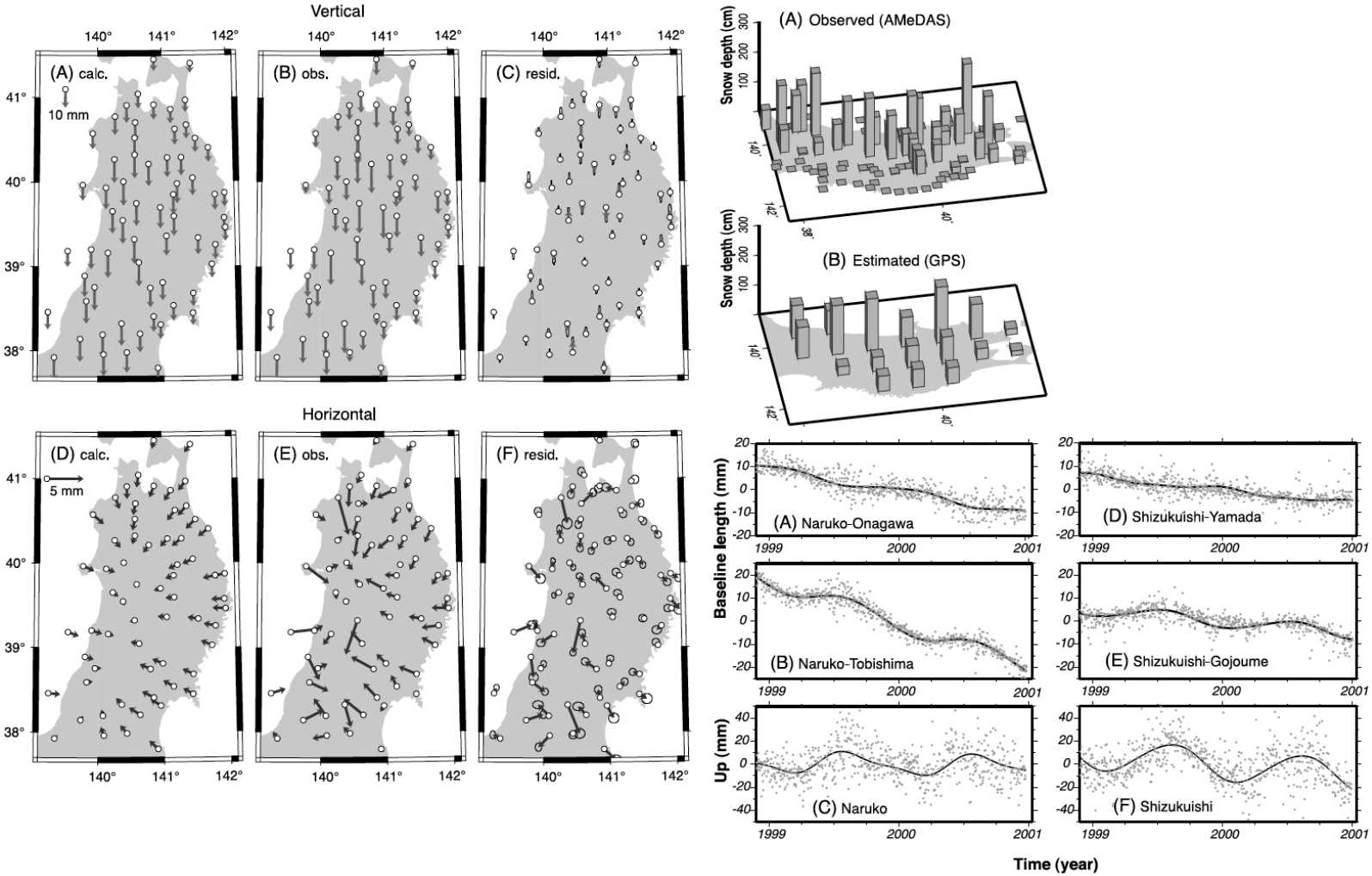

Heki 2001, Science

Applications – Snow Depth

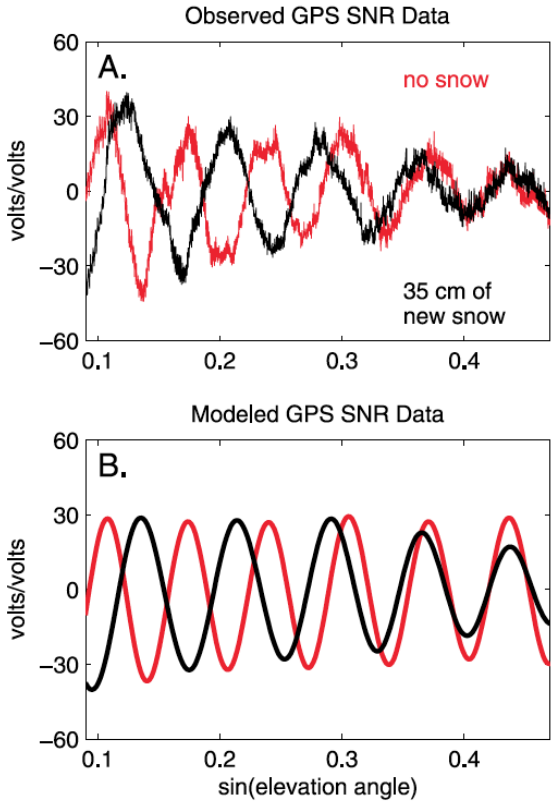

Figure 1. (a) GPS SNR measurements for PRN 7 observed at Marshall GPS site on days 107 (red) and 108 (black) after direct signal component has been removed (see text). Approximately 35 cm of snow had fallen by day 108. (b) Model predictions for GPS multipath from day 107 with no snow on the ground (red), and day 108 after 35 cm of new snow fall had accumulated (black) using an assumed density of 240 kg m^{-3}.

Left: McCreight et al. 2014, Water Res.; Right: Larson et al. 2009, GRL

Applications – Vegetation Growth

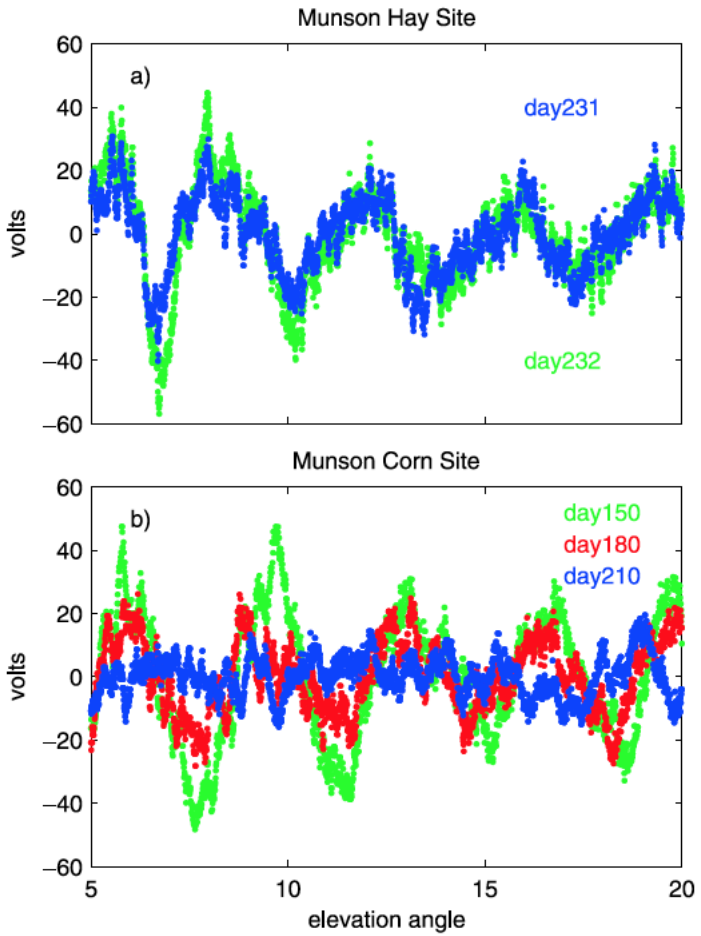

Figure 2. (a) SNR data for hay field before (day 231) and after (day 232) the field was mowed; (b) SNR data for no corn (day 150), 50 cm corn height (day 180), 2 m corn height (day 210). In addition to the effects of vegetation highlighted here, multipath amplitude decreases as the satellite rises because of the antenna gain pattern.

Left: McCreight et al. 2014, Water Res.; Right: Larson et al. 2009, GRL

Applications – Volcanic Ash Plumes

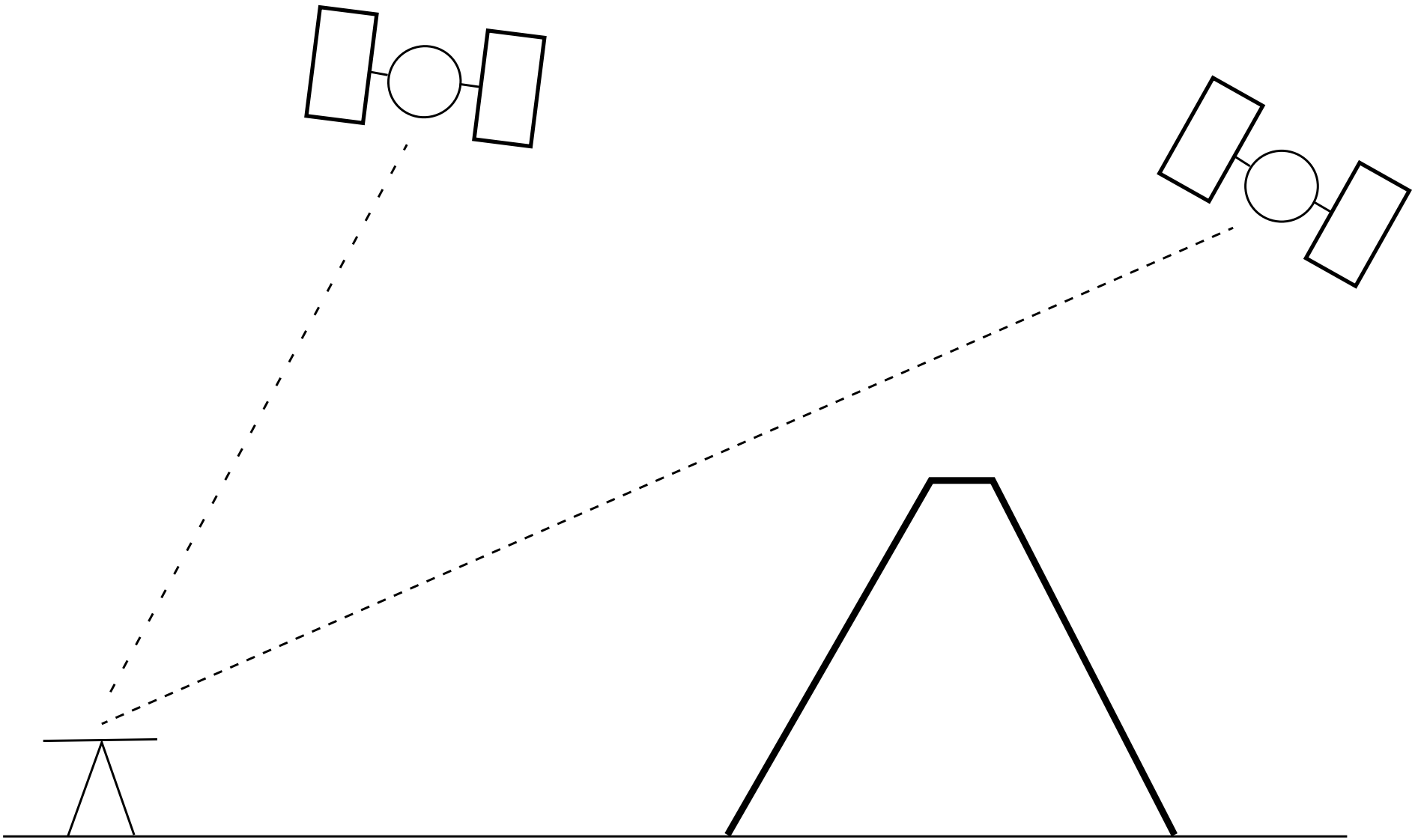

Applications – Volcanic Ash Plumes

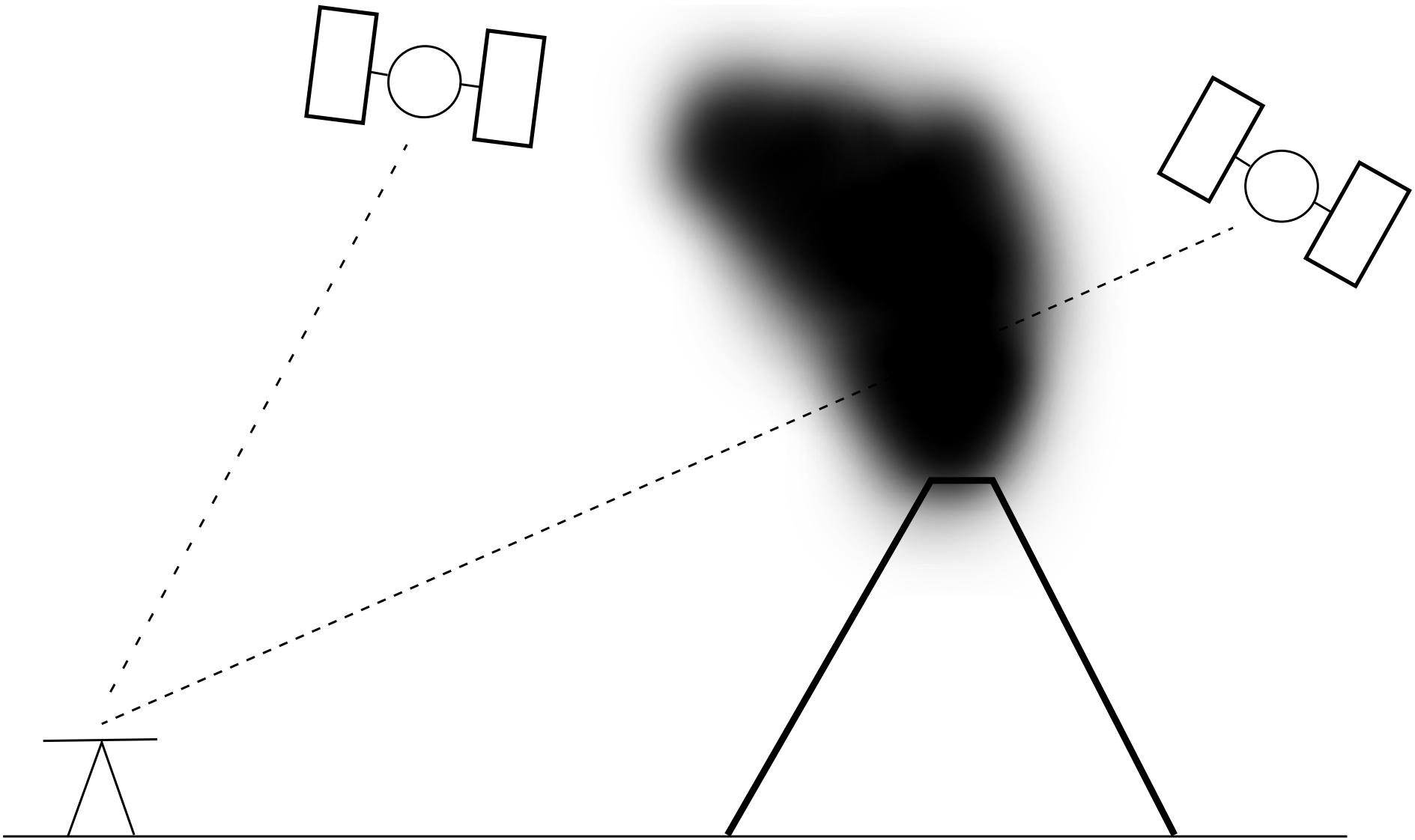

Applications – Volcanic Ash Plumes

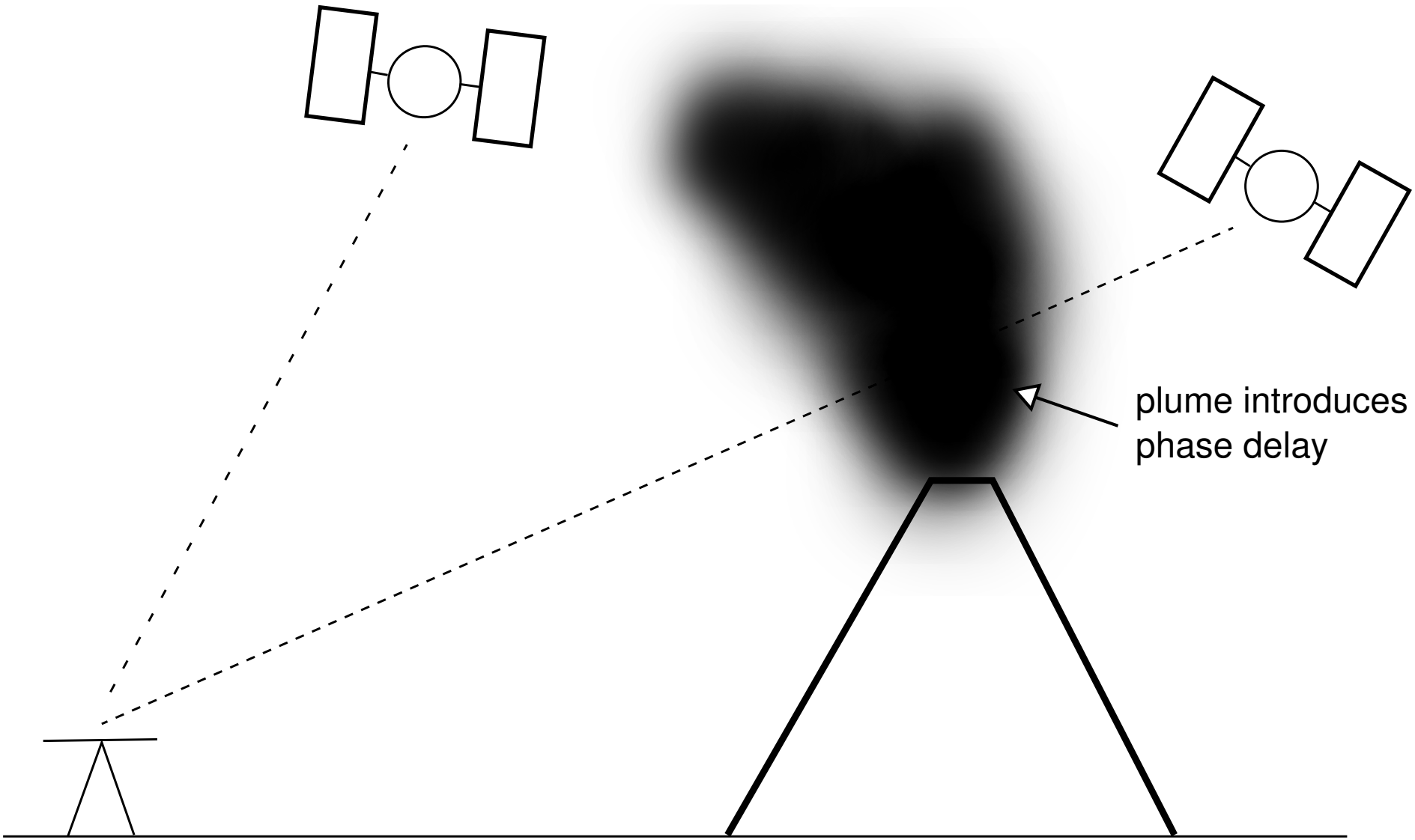

Applications – Volcanic Ash Plumes

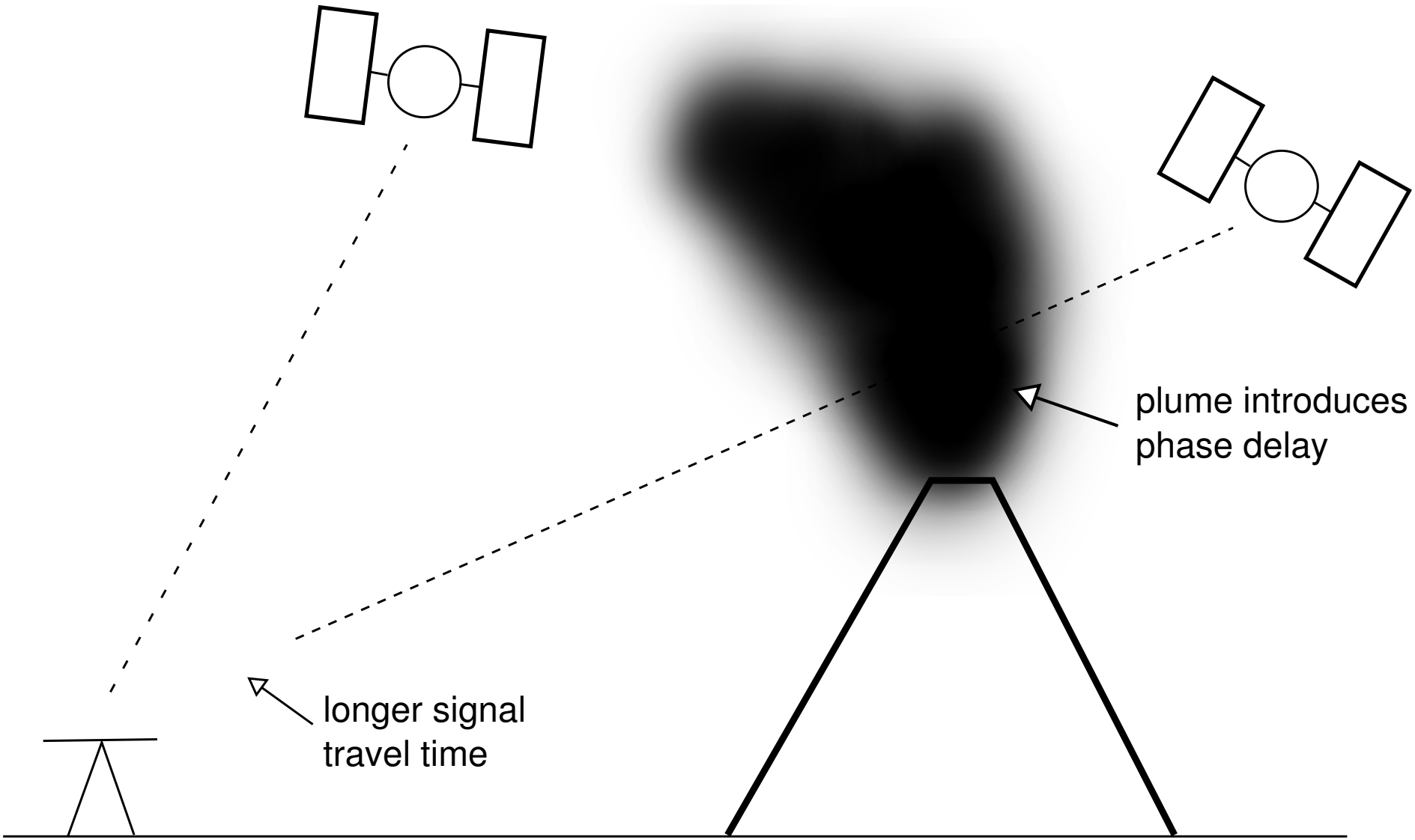

Applications – Volcanic Ash Plumes

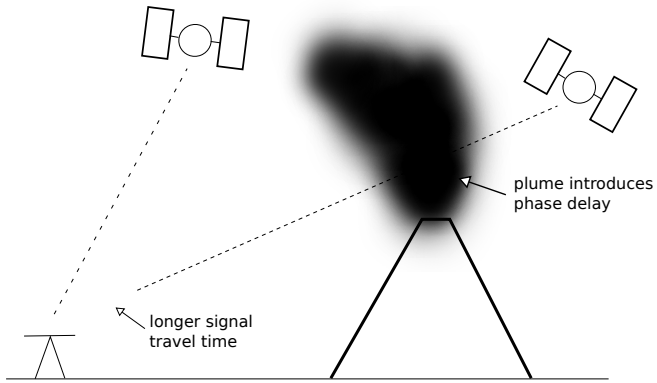

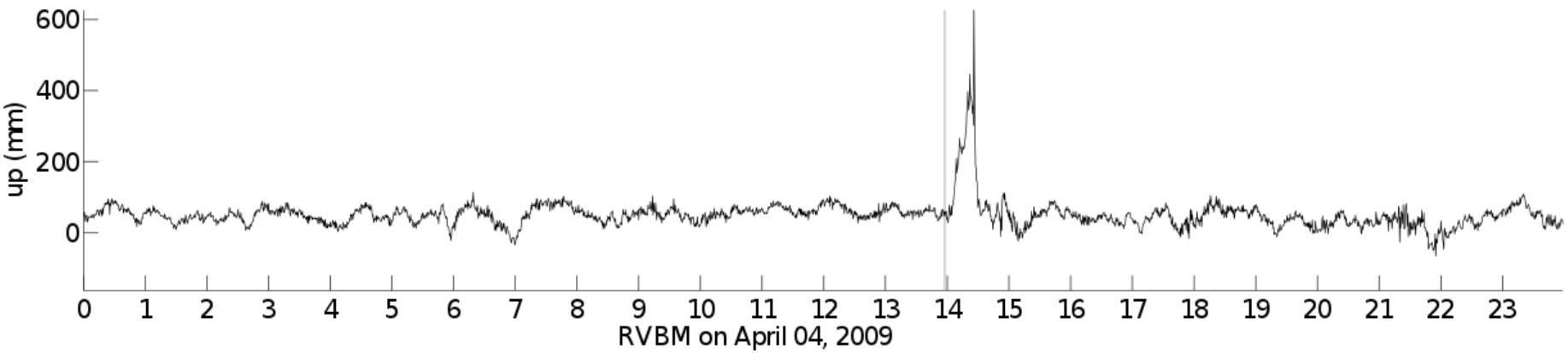

Applications – Volcanic Ash Plumes

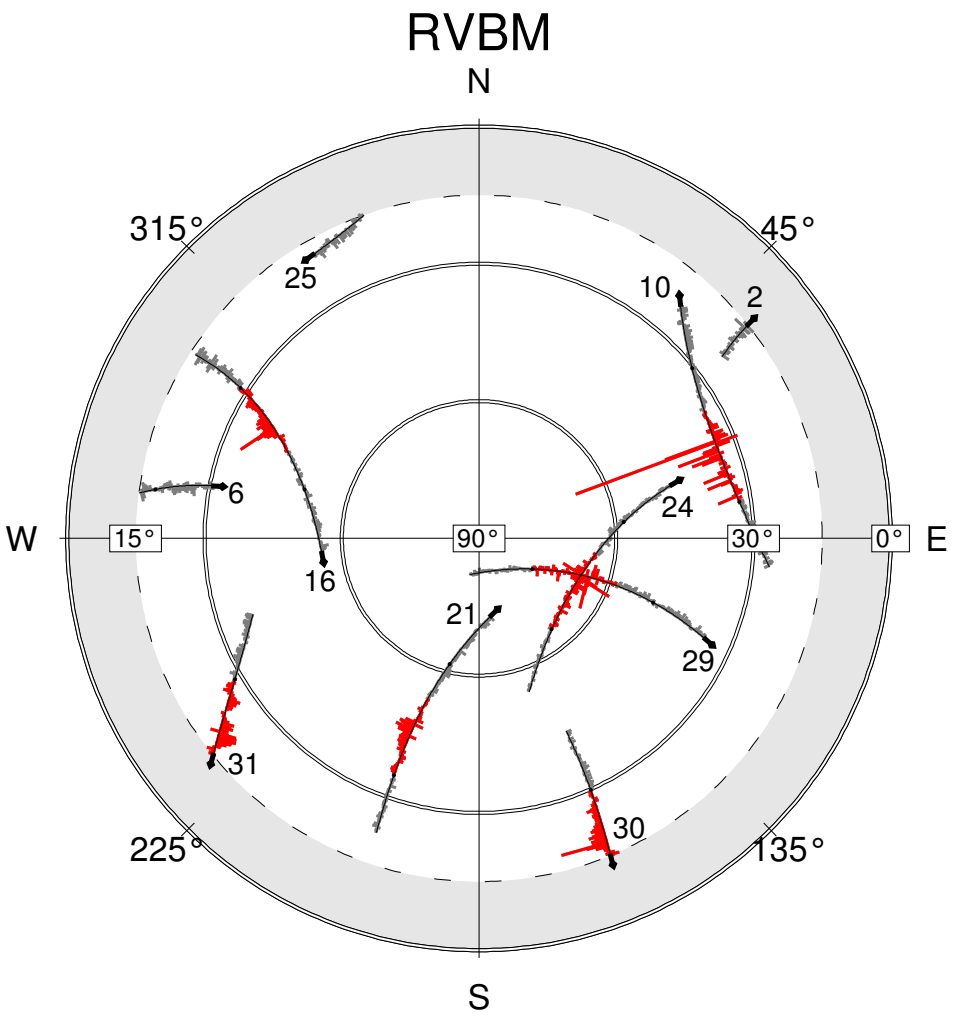

Explosion: 04 April 2009, 14:00 to 14:40 UTC

Grapenthin et al., JVGR (2013b)

Applications – Volcanic Ash Plumes

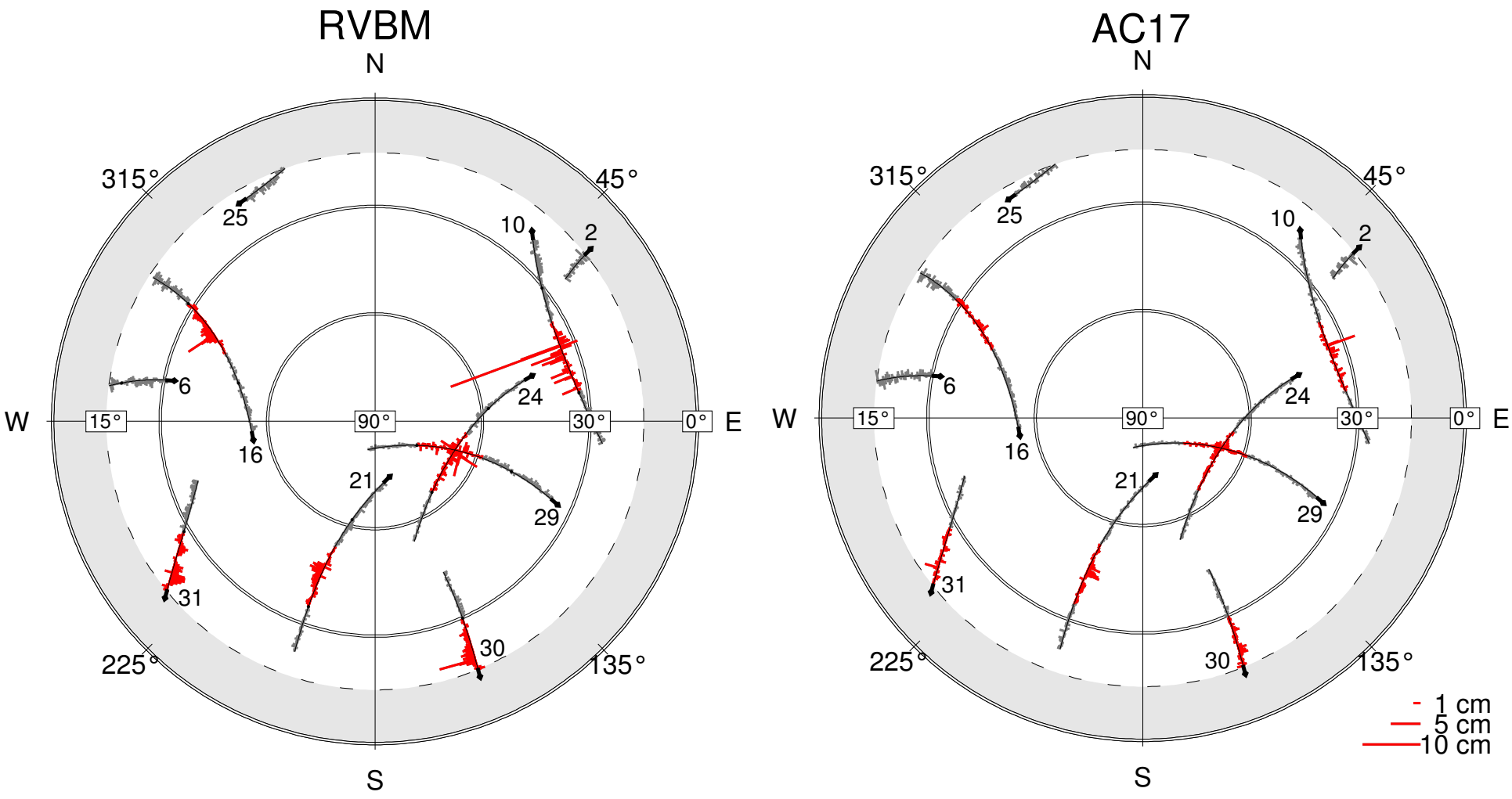

Explosion: 04 April 2009, 14:00 to 14:40 UTC

Grapenthin et al., JVGR (2013b)

Applications – Volcanic Ash Plumes

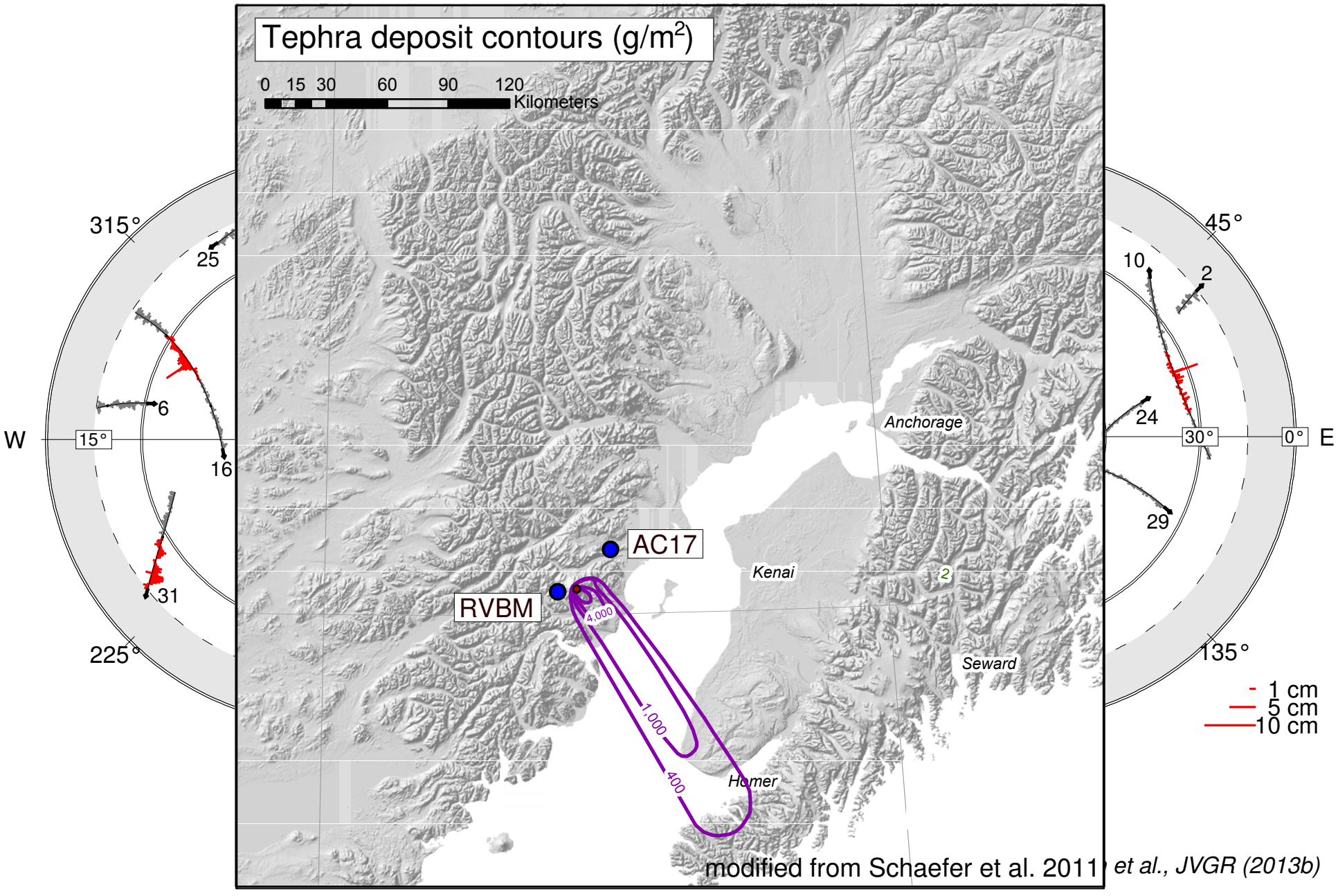

Applications – Volcanic Ash Plumes

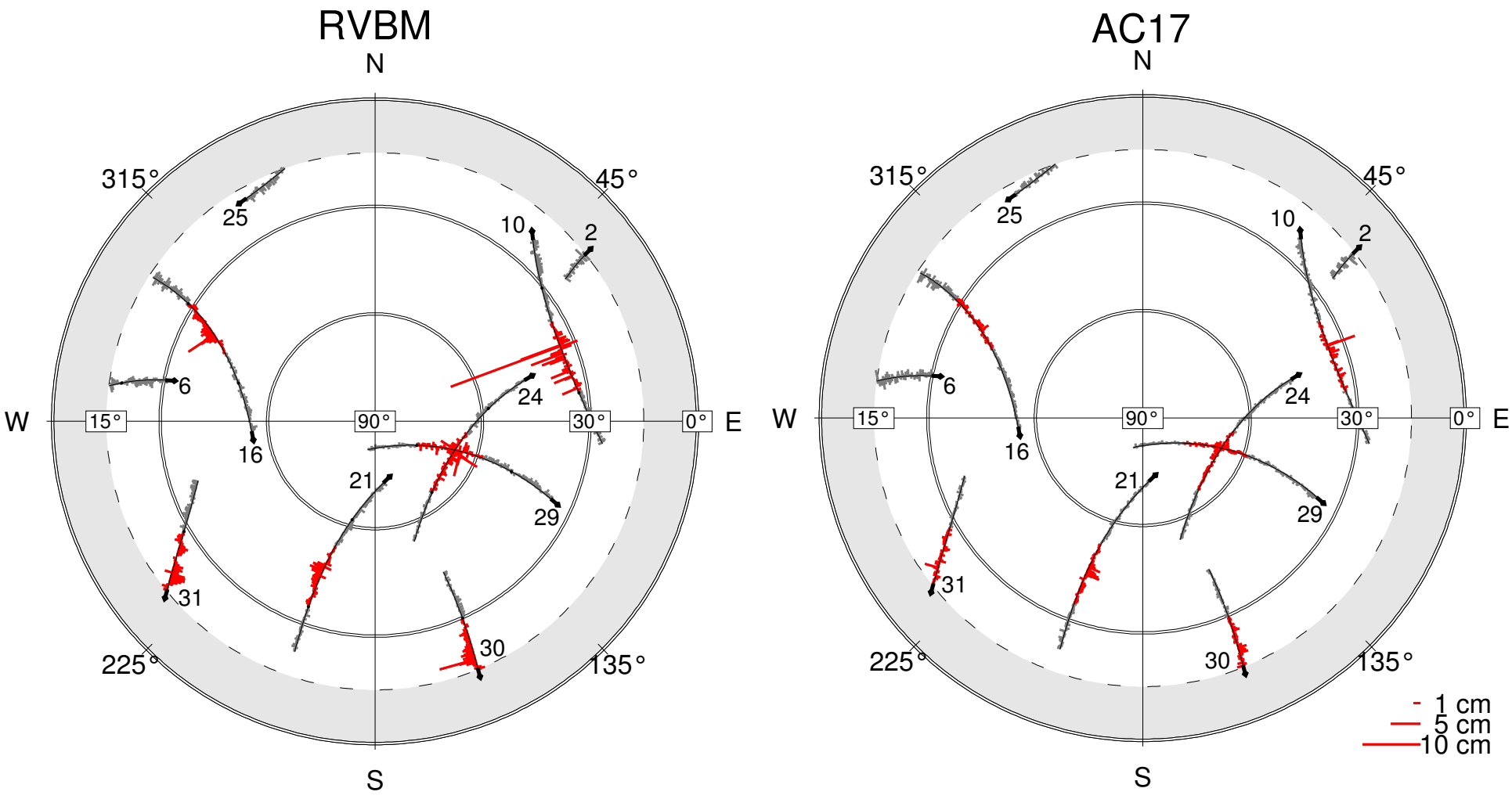

Explosion: 04 April 2009, 14:00 to 14:40 UTC

Grapenthin et al., JVGR (2013b)

Applications – Volcanic Ash Plumes

RVBM – AC17

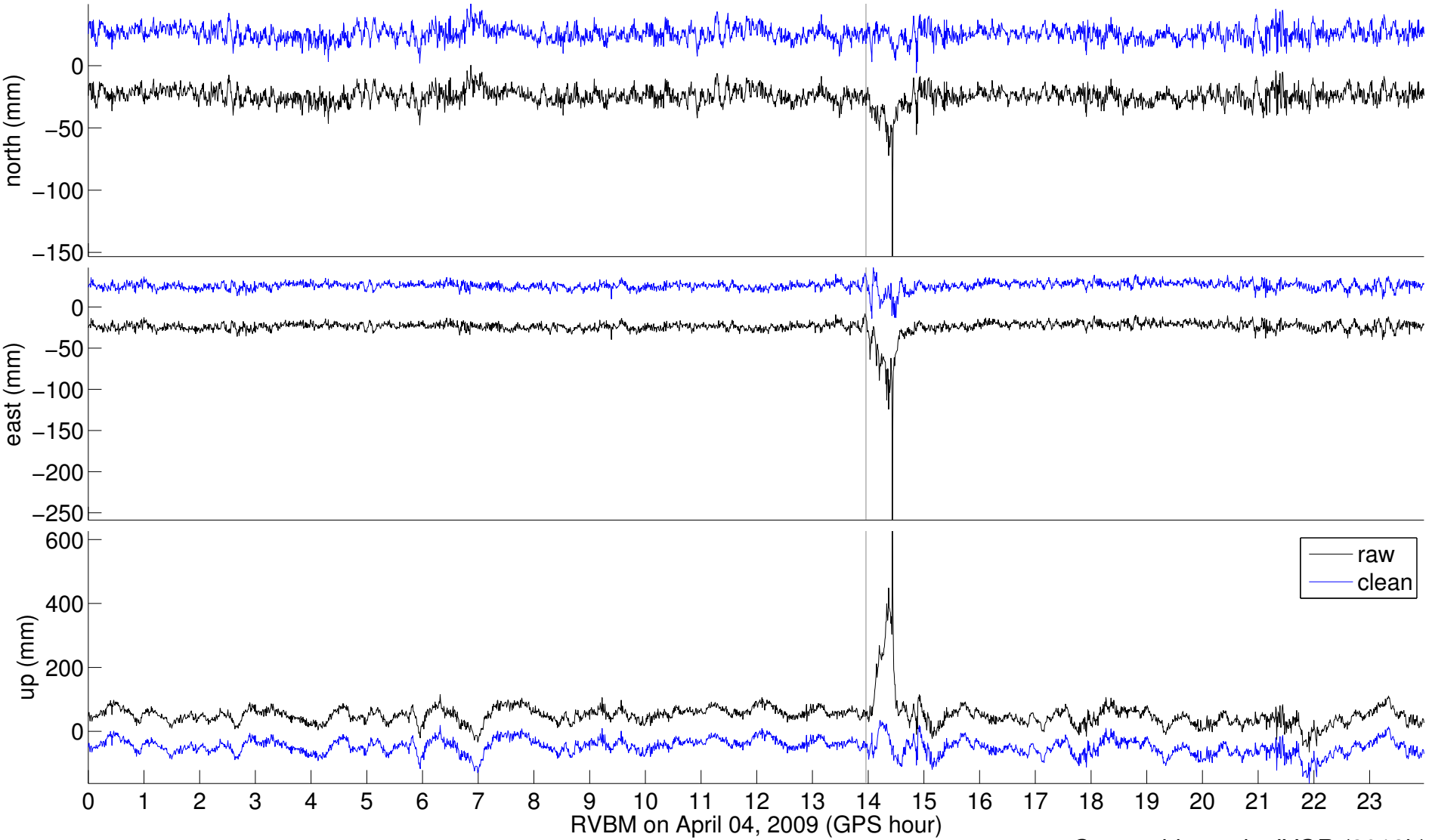

Grapenthin et al., JVGR (2013b)

Applications – Volcanic Ash Plumes

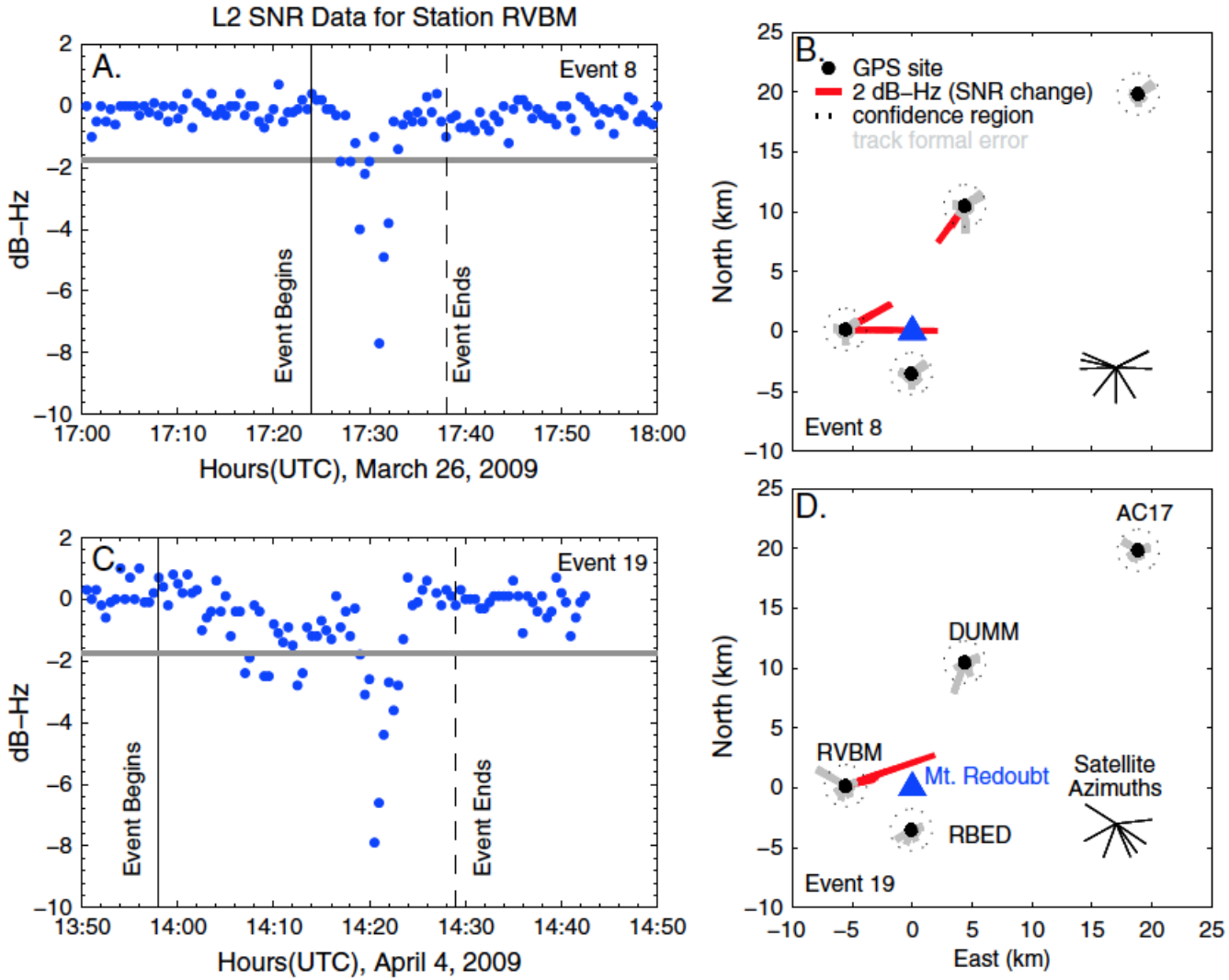

Figure 3. (a and c) SNR data for GPS station RVBM and events 8 and 19. Eruption times are determined with seismic sensors [*Bull et al.*, 2012]. Nominal detection level is shown as the horizontal gray line. (b and d) Summary mapview representation of plume detections. Gray lines at four stations (black circles) indicate nondetections for satellites transmitting from those azimuths. Red lines indicate significant plume detections (scale given).

Larson 2013, GRL

Applications – GNSS Meteorology

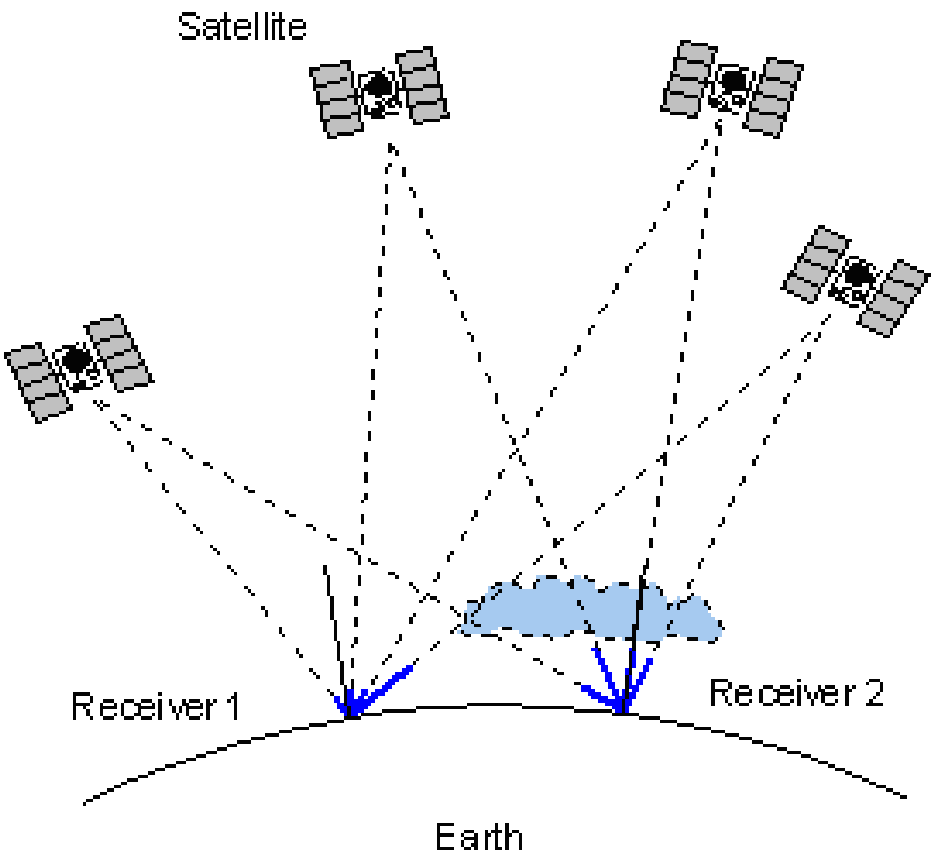

Observed delay

computed hydrostatic delay

$$T = (M_d(e) * T_d^z) + M_w(e) * T_w^z$$

Known mapping function

Unknown tropospheric zenith wet delay

Applications – GNSS Meteorology

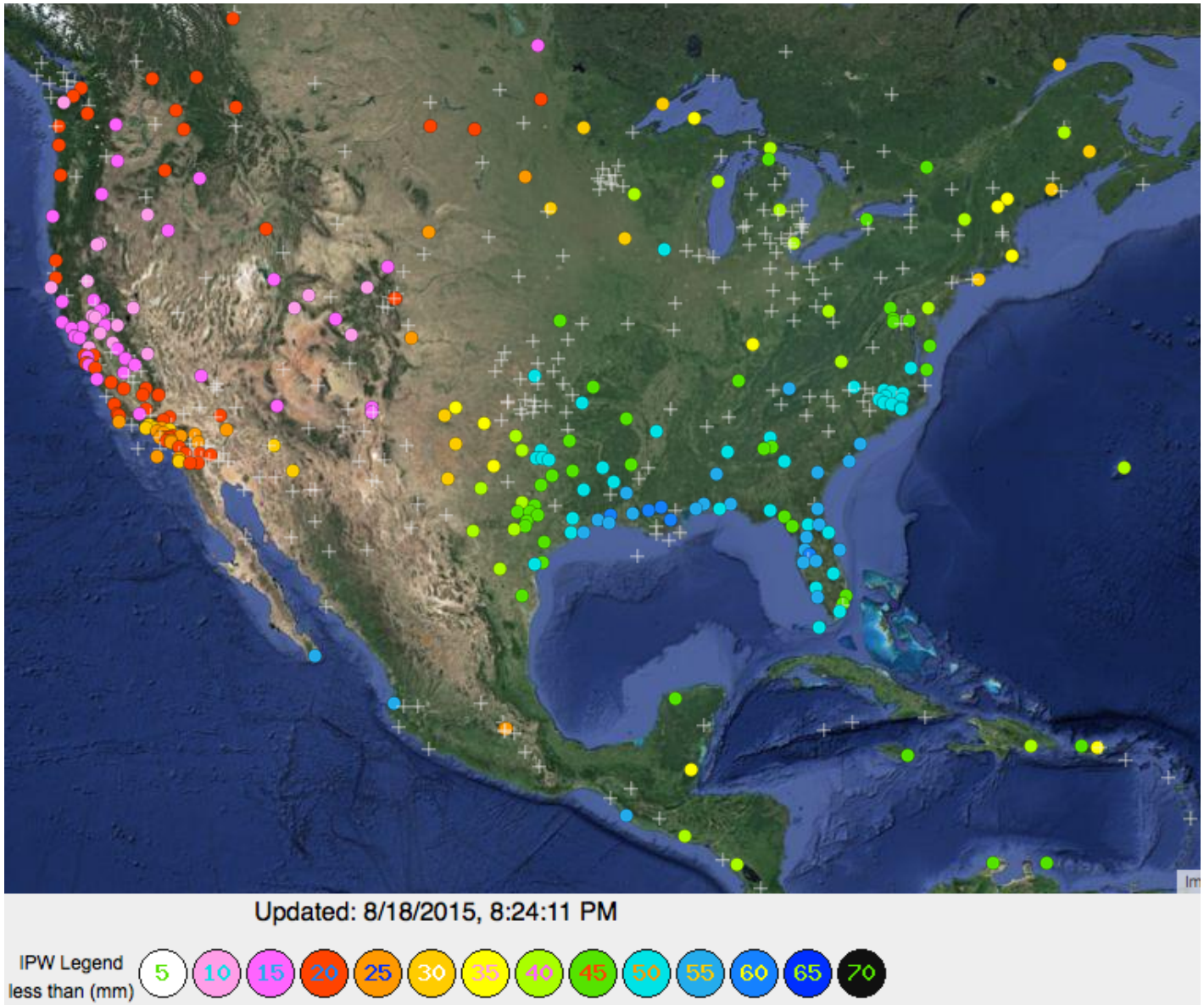

source: `http://www.gpsmet.noaa.gov/`

Applications – GNSS Meteorology

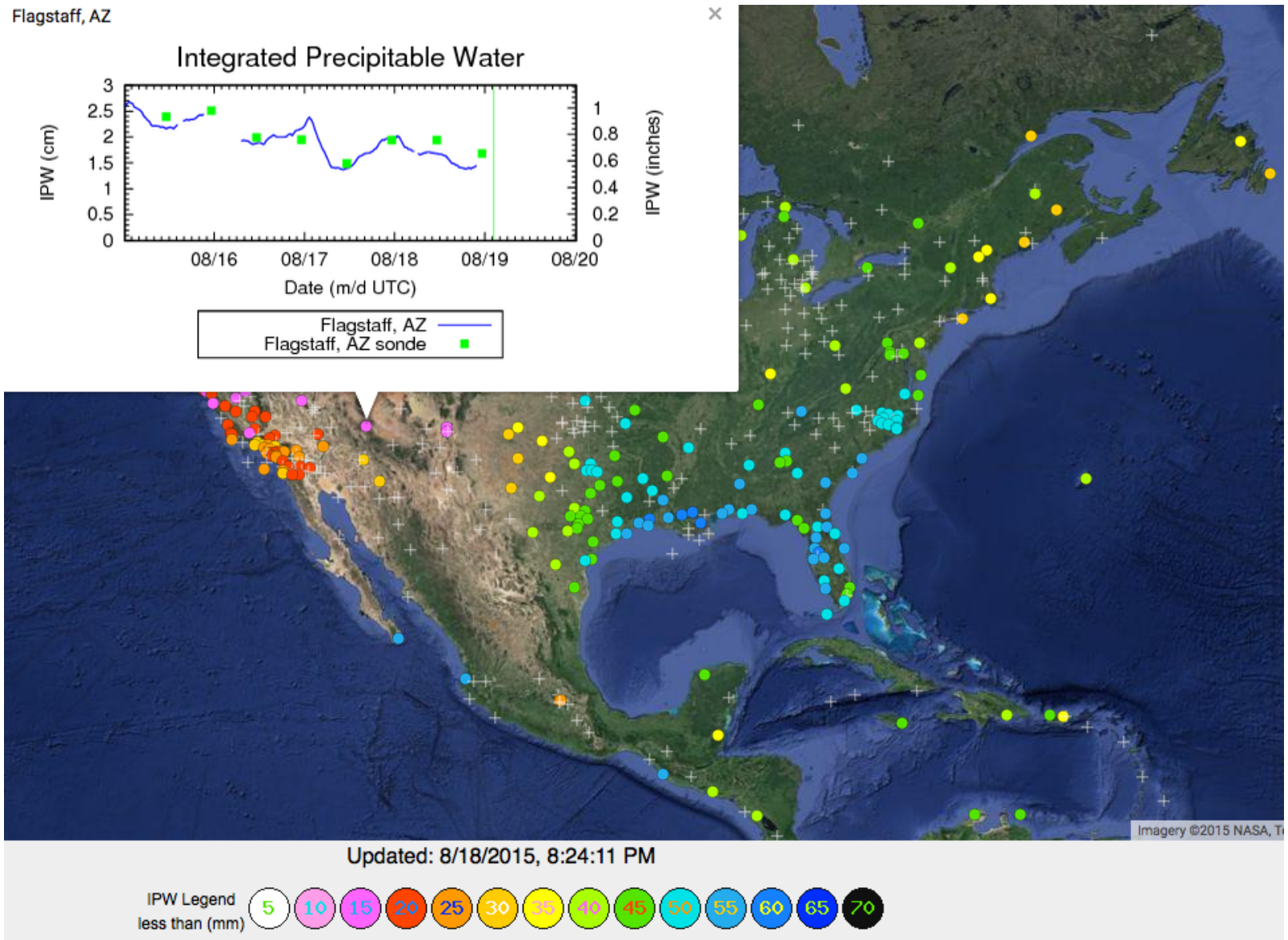

source: `http://www.gpsmet.noaa.gov/`

Applications – GNSS Meteorology

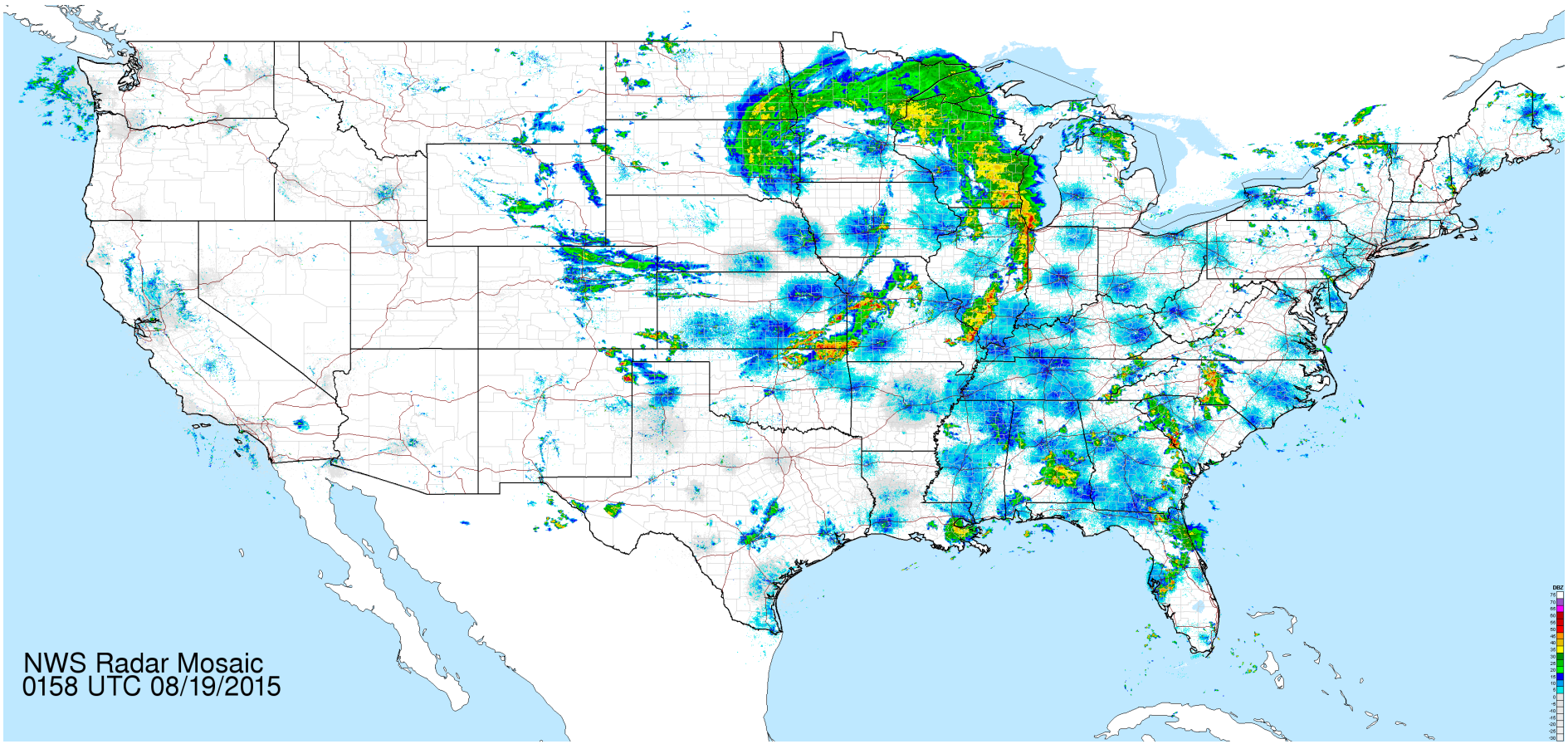

source: `http://www.radar.weather.gov/`

Applications – Ionosphere Studies

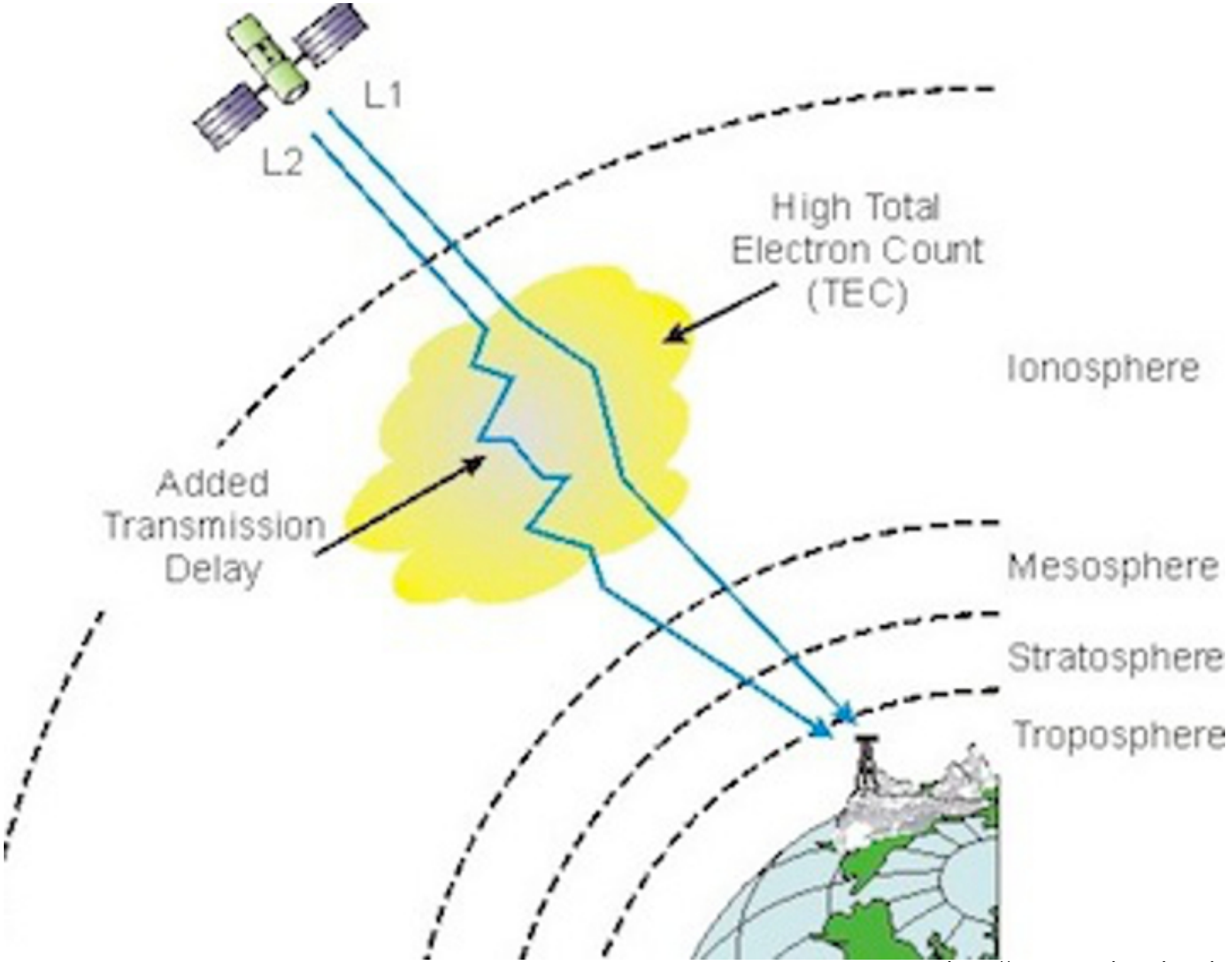

source: http://xenon.colorado.edu/spotlight/

Applications – Ionosphere Studies (Tsunami EW)

NASA / JPL Tohoku Ionosphere movie

NASA/JPL-Caltech, video doesn't work? try: `https://www.youtube.com/watch?v=17GNzXmEYjA`